AIR FORCE ACADEMY

Structural Improvements of a FishBAC Design

Tiago Emanuel Pereira Nunes

ALFAL/ENGAER 139923-D

Thesis to obtain the Master of Science Degree in

Military and Aeronautical Sciences - Aeronautical Engineering

Examination Committee

Chairperson:	BGEN/ENGAER 086084-A João Rui Ramos Nogueira
Supervisor:	Prof. Benjamin King Sutton Woods
Co-Supervisor:	TCOR/ENGAER 129905-A Luís Filipe da Silva Félix
Member of the Committee:	Prof. Frederico José Prata Rente Reis Afonso

Sintra, December 2022

To my family and friends

Acknowledgments

To my parents, for all the support they gave me, as well as all the love and pride they always had for me, never forgetting the education they gave me.

To my sister Bruna and my friend Filipa that, even if distant, were always available to help in professional and emotional terms.

To all my teachers and educators, from kindergarten through Abambres Primary School, Diogo Cão Basic School, Morgado de Mateus School and Camilo Castelo Branco School, to whom I owe a lot for their contribution to my personal and professional development. To my girlfriend Daniela for the emotional support and the enormous patience she showed in the course.

To my course mates who helped me in this journey and whose friendship I will keep for the rest of my life. I would also like to thank, in a more remarkable way, my speciality colleagues António Oliveira, Raquel Rocha and Tirsa Arriscado for the help and good mood they provided, even in difficult situations.

To Professor Benjamin King Sutton Woods who, since the first contact that we had, showed himself available to help in the development of this dissertation.

To Lieutenant Colonel Luís Félix for his tireless patience, understanding and help provided throughout the course.

To all those who, in various ways, have passed through my life, contributing to my personal, social and professional improvement.

To all my sincere thanks.

Resumo

A indústria aeronáutica é conhecida pela sua elevada exigência. Actualmente, essa exigência é cada vez mais notória, o que leva à procura ativa de ideias e soluções que sejam inovadoras, criativas e mais eficientes para a continua evolução do desempenho das aeronaves. Uma das novas e promissoras ideias é a asa do tipo *Fish Bone Active Camber* (FishBAC), que se insere na categoria de asas que tem uma curvatura variável consoante o pretendido. Neste trabalho, propõe-se novas soluções que possam responder às limitações dos modelos atuais da tecnologia FishBAC.

Como mecanismo adaptativo (*morphing*) baseado na flexibilidade, a distribuição e orientação da rigidez dentro do FishBAC são incrivelmente importantes. O objectivo geral é conseguir uma elevada flexibilidade na direcção da curvatura variável mantendo, simultaneamente, uma elevada rigidez nas outras direcções. A geometria do FishBAC foi projetada para criar um elevado nível de anisotropia estrutural. Este trabalho procura levar esta estrutura mais longe, investigando uma série de alterações de concepção que irão aumentar ainda mais a anisotropia geométrica e dos materiais utilizados, de modo a aumentar o desempenho do FishBAC .

Estas soluções foram obtidas usando três modelos diferentes. O primeiro modelo apresenta recortes rectangulares na espinha (*spine*). O segundo tem pultrusões de polímero reforçado com fibra de carbono (*Carbon fiber reinforced polymer* - CFRP) presas às longarinas e colocadas junto à pele (*skin*). E o terceiro modelo combina as características dos outros dois. Os resultados de uma análise de elementos finitos (*Finite Element Analysis* - FEA), obtidos para estes modelos, foram comparados a um modelo básico FishBAC sem modificações. Concluiu-se que os recortes têm um efeito positivo na diminuição da rigidez do modelo, com um impacto modesto na variação da deflexão do bordo de fuga, ao longo da envergadura. As pultrusões de CFRP demonstraram ser muito menos eficazes para responder ao problema da elevada variação da deflexão do bordo de fuga do que seria de esperar para estruturas quem incluem este tipo de reforços (pultrusões de CFRP).

Palavras-chave: Análise de Elementos Finitos; Modelo Computacional; Asa Adaptativa; FishBAC, Fibra de carbono reforçada com polímero.

Abstract

The aeronautical industry is well known for its high demands. Nowadays, the demands are higher and more visible, which leads to the active search of new ideas and solutions that are innovative, creative and more efficient for the continuous evolution of the aircraft's performance. One of these new and promising ideas is the Fish Bone Active Camber (FishBAC) wing, which is a type of camber morphing wing. This dissertation work proposes new solutions that aim to mitigate the limitations of the current models of the FishBAC technology.

As a compliance-based morphing mechanism, the distribution and orientation of stiffness within the FishBAC are incredibly important. The overall goal is to achieve high compliance in the camber morphing direction while maintaining high stiffness in the other directions. The geometry of the FishBAC is designed to create a high level of structural anisotropy. This work seeks to push this structure further by investigating a series of design changes which will further augment the material and geometric anisotropy in order to increase the performance of the FishBAC.

These solutions were obtained using three different models. The first model presents a spine with rectangular cutouts. The second one has Carbon Fibre Reinforced Polymer (CFRP) pultrusions attached to the stringers next to the skin. The third model combines the characteristics of the other two. The results obtained through the Finite Element Analysis (FEA) for these models, were compared to a basic FishBAC model with no modifications. This process helped to conclude, that cutouts have a positive effect in diminishing the stiffness of the model with a modest impact in deflection variation along the wingspan. The CFRP pultrusions have shown to be much less effective to respond to this deflection variation problem than it was expected.

Keywords: FEA, CAD, Morphing Wing, FishBAC, CFRP

Contents

List of Figures

List of Tables

Abbreviations

ABS Acrylonitrile Butadiene Styrene

AHP Analytic Hierarchy Process

CAD Computer Aided Design

CFRP Carbon Fiber-Reinforced Polymer

DE Dielectric Elastomer

EMC Elastomeric Matrix Composite

FEA Finite Element Analysis

FEM Finite Elements Method

FFF Fused Filament Fabrication

FishBAC Fish Bone Active Camber

GATOR Geometrically Anisotropic Thermoplastic Rubber

MAW Mission Adaptive Wing

MFC Macro-Fiber Composite

SABRE Shape Adaptive Blades for Rotorcraft Efficiency

SMA Shape Memory Alloys

TPU Thermoplastic polyurethane

UAV Unmanned Aerial Vehicle

UD Unidirectional

Nomenclature

Greek symbols

Δ_{norm} Absolute difference between the maximum and minimum displacements normalised by the average displacement.

ϵ Linear Strain.

γ Rotational Strain.

ν Poisson's ratio .

ν_{12} In-plane Poisson's ratio .

σ Linear Stress.

σ_P Population Standard Deviation.

τ Shear Stress.

Roman symbols

b Wing span.

c Wing chord.

C_D Coefficient of drag.

C_L Coefficient of lift.

E Young's modulus.

E_{11} Young's modulus in the fibre-direction.

E_{22} Young's modulus in the matrix-direction.

G Shear modulus.

n Total number of points .

S Compliance Matrix.

T Torque.

w Deflection.

$\bar{w}$ Average deflection.

$w_{s/2}$ Deflection at span midpoint.

Subscripts

max Maximum value.

min Minimum value.

Chapter 1

Introduction

This section presents the motivation for this research and its objectives. It also briefly describes the structure of the thesis.

1.1 Motivation

Aviation is one of the most important fields worldwide. In the military sector, it is one of the main forces and its impact and power are beyond any argument. Therefore, the continuous development and evolution based on new and future technologies is of extreme importance.

An aircraft itself is already an extreme complex system but it gets even more complex in the military aviation sector, due to its design and the requisites that it needs to fill (Biswas, 2020). Optimising and improving its performance on several possible mission scenarios is indeed a challenge (Vasista, Tong, & Wong, 2012). It becomes more and more important the collaboration and development of technologies alongside the evolution of the aviation field, as the most recent technologies give the possibility to change and improve design, instruments and other parts of the aircraft (Esposito & Raffa, 2007). This can be a great asset for aviation as it can lead to great advantages in military missions and operations.

Considering the above, camber morphing wings are a promising way of accomplishing the performance needs of an aircraft, since these structures are much more aerodynamic efficient than conventional devices, such as ailerons, elevators and trailing edge flaps (Rivero et al., 2020). This can provide the lift needed for different stages of the aircraft operations with less drag and noise, usually associated to hinged control panels (Rivero, Weaver, Cooper, & Woods, 2018). Besides these advantages, these types of morphing devices have a critical point that needs to be considered which is the complexity and weight associated. Making sure that these factors do not significantly influence the structure's feasibility is one of the major challenges when designing these devices.

The motivation behind this study is to improve aircraft performance by means of camber morphing wings, with the FishBAC technology. This will make the wings more capable of having a better performance when applied to an aircraft, that can operate several different missions, for instance, an Unmanned Aerial Vehicle (UAV) that can be operated by the Portuguese Air Force.

1.2 Objectives and Deliverables

The purpose of this dissertation is to explore new ideas and concepts that can make the camber morphing mechanism more structurally efficient. This will be done throughout the study of the structural behaviour of a FishBAC device. The study of structural efficiency will focus on minimising elastic washout between actuation stations, while trying to maintain or even diminish the complexity and total mass of the structure.

Another goal of this work is to provide computational models that support further research on the structural optimization of the FishBAC device with the application of potential modifications to the structure. In order to achieve those objectives, Computer Aided Design (CAD) modelling and FEA will be used to evaluate the designed structure and give important information that can support the conducted study.

1.3 Thesis Outline

The present thesis is structured in the following manner.

The first chapter (chapter 1) gives the reader an overview of the subject, as well the motivation and the main objectives for development of this study.

Chapter 2 contextualizes the study by introducing the concepts and procedures necessary to perform the FEA. Here, it is also reviewed the existing technologies related to camber morphing wings and the evolution of the FishBAC, showing the three generations of this morphing wing device developed so far.

Chapter 3 describes the decision process and the results proceded by it. In this chapter, the CAD representation of the FishBAC is shown, the structural test and the respective analysis are developed, delivering a baseline model to use as a reference for the following studies.

Chapter 4 presents and discusses proposed structural design changes, including the CAD models studied and the mechanical tests done (same tests as those done to the baseline model), as well as its results.

The last chapter 5 provides a conclusion of all the work done, as well as its limitations and suggestions for future work.

Chapter 2

Fundamental Concepts and State-of-the-Art

2.1 Structural Analysis

2.1.1 Structural Concepts

The main subjects of this dissertation are the morphing wings and the FishBAC morphing concept. Before diving into the main subject, it is important to contextualise and define the basic structural and material concepts, in order to perform a better and understandable structural analysis.

Raymer (2018) mentioned that the deformation of a body, after applying an external load, will tend to a value that can assure the equilibrium of the internal forces of that body. When dividing these forces (F) by the section area (A) where these are present, it is obtained the stress (σ), and the deformation caused by this stress, when dimensionalized by the original dimension of the body, is defined as strain (ϵ) (Beer & Johnston, 2012). The applied forces can be categorized as compression, tension and shear, whereas the applied moments are defined as bending and torsion. It is also important to mention that Poisson's ratio ν is defined by Hibbeler (2017) as the relation between a transversal/lateral and a longitudinal/axial strain of a body, when an axial load is applied.

Brandt, Stiles, Bertin, and Whitford (2015) referred that the applied load and the obtained stress for that load have a proportional relation, when considering the linear elastic behaviour range of the material being studied. This is known as Hooke's Law and, for cases where the material is in tension or compression, the relation is given by Equation 2.1, where E represent Young's modulus and ϵ stands for strain. If the material is in shear, the relation is given by Equation 2.2. In this latter equation, the γ refers to the rotational strain, τ to the shear stress and G the Shear modulus.

$$\frac{F}{A} = \sigma = E \cdot \epsilon, \tag{2.1}$$

$$\tau = G \cdot \gamma, \quad G = \frac{E}{2(1+\nu)}. \tag{2.2}$$

It is important to mention that Equations 2.1 and 2.2 are only possible to be applied if the material is isotropic. This term refers to materials that, no matter the direction considered, all of its properties are equal (Roylance, 2000). On the opposite side, if a certain material is called anisotropic, it means that all properties are different for all the directions of the material.

The characterisation of an orthotopic material is also important for the work developed for this dissertation. The isotropic has an infinite number of symmetry planes whereas an anisotropic material has no symmetry planes. The special case between these two types of material is the orthotropic which has two planes of symmetry where material properties are independent of the direction within each plane. Barros (2018) mentions that for an orthotropic material, the shear stresses in a certain direction, only originate deflections in the exact plane that is being applied. This is supported by the fact that the Compliance Matrix S (Reddy, 2003) is symmetric for this type of material. Laminate composite materials with low thickness are considered orthotropic and, as each lamina can be considered homogeneous from the macroscopic point of view, it is possible to apply Hooke's Law to this type of material (Ramos, 2015).

2.1.2 Numerical Method using Finite Elements Analysis (FEA)

The capability that computers have to generate and calculate massive batches of numbers in a relatively short time, when compared to human computation, has helped with the progress of many scientific areas, including mechanics. Doing a structural analysis using analytical methods is only feasible for simple models and not for complex ones. A computational process can be a reliable solution if the model and analysis method used are appropriate to the structure being studied. If this is not verified the numerical errors can present a considerable dimension and be higher than the analytical errors. It is also true that the computational method is much easier and possible to obtain, in a much faster way, when compared to the experimental method. It is important to mention that the reliability and precision of the computational results are only accessed by having a comparison made with the experimental results for the same type of testing.

In this line of thought, FEA is a numerical tool that can help to study complex structures, with the possibility of its optimisation with less cost, when compared to experimental work, which is always an important factor, and much faster (Brandt et al., 2015). This tool divides the continuous structure into small discrete elements, transforming the structure that has an infinite number of degrees of freedom into a finite number.

To be able to start a FEA it is necessary to do a CAD of the structure that is going to be studied, which will be later divided into these small discrete elements. These elements can have two or three dimensions and have multiple nodes. Mesh is the designation used to describe a group of elements.

One other step in this progress is to define the material properties of each component of the structure. These material parameters explained in Chapter 2.1.1, are related to elements and their type. The next step of the FEA is to define a simulation, the closest to the mechanical situation that the structure is designed to support. This requires the definition of the specific loads that are applied, the boundary conditions and spacial restrictions.

As the last step, a process of verification and validation must be carried out, analysing if the parameters of the solution (displacements, stress, strains, buckling, etc.) are in agreement with the expected behaviour for that specific parameter. There are some cases where there is no reference to the expected behaviour has it is difficult to predict it. So for this type of case, an experimental test must be done with the obtained results being used as a reference for the validation of the computational ones.

If the results are not validated, a re-design and a new FEA process must be carried out.

A summary of the FEA process is presented in Figure 2.1

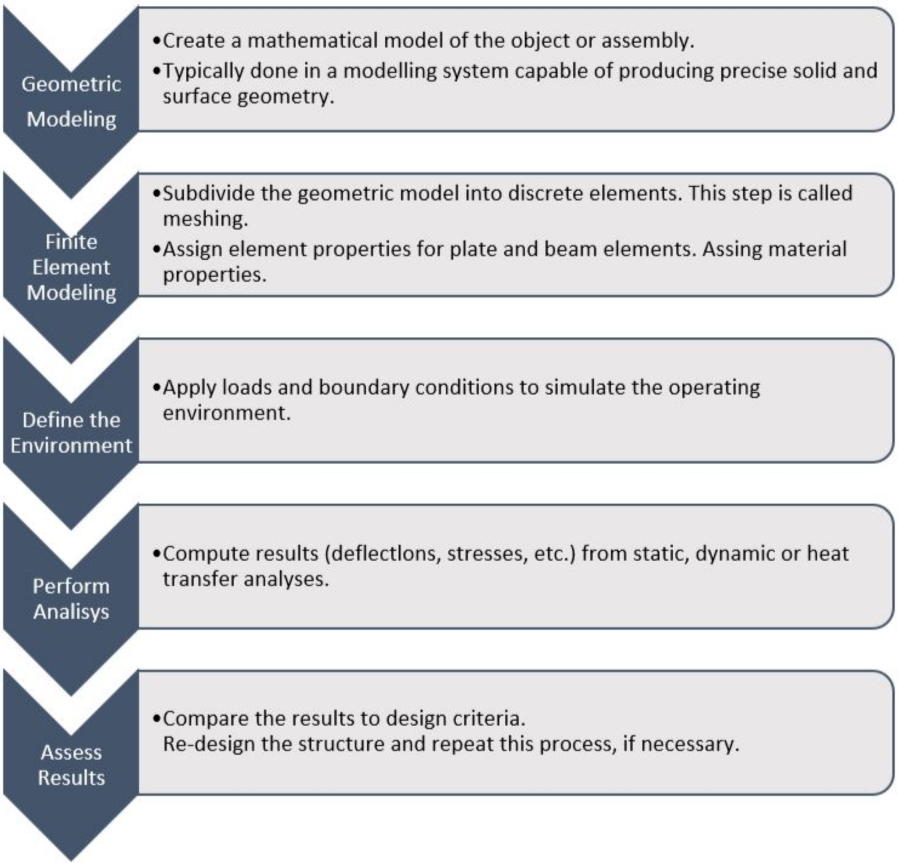

Figure 2.1: Summary of the FEA process (adapted from Niu, 1999).

It is also important to mention that the type of analysis considered for this work was linear static. In this regime, an increase or decrease of the applied loads results in a proportional increase or decrease of the respective deformations because the stiffness is constant. In practice, this is applicable to structural problems where stresses remain in the linear elastic range of the used material, which is the case of this work.

Usually, the software that runs the FEA analysis does a gradual increase of the applied load's value, until it reaches the total magnitude. This happens in order to be possible to disregard the damping forces involved (Systèmes, 2017).

2.2 Camber Morphing Wings

There is no clear and simple definition for the term morphing wings. However, morphing is a term used in the science of aeronautics to describe an aircraft or a specific part of it that undergo certain geometrical modifications, to perform better considering the mission requirements. Despite this, as Sofla, Meguid, Tan, and Yeo (2010) explained, there is a consensus that traditional hinged control surfaces or high lift mechanisms, such as flaps or slats, which offer discrete geometry changes, cannot be regarded as ”morphing”. Taking this into consideration it can be defined that wings with camber morphing capabilities can modify geometrically to achieve a certain camber. This parameter is extremely important to flight as it influences the lift and drag produced by the wing.

Rivero et al. (2018) mentions that the lift coefficient (C_L) needed to maintain flight changes depending on the flight stage. This crucial lift coefficient is determined by variables, like aircraft weight (that can change throughout the flight), altitude, atmospheric conditions, and manoeuvres. The variations in C_L can currently be produced via one of two primary methods: modifying the camber distribution or altering the angle of attack of the entire aircraft. The former method can be accomplished, in a discrete way, with conventional control surfaces and high lift devices, composed of hinged panels attached to the main wing (e.g., ailerons, elevators and trailing edge flaps). Although the lift force effectively varies because of the deflection of these hinged panels, the abrupt change in the aerofoil section results in a large drag penalty and noise. This makes them an unattractive alternative for more ambitious attempts to actively and constantly modify the camber of the entire wing.

Another advantage of employing camber morphing devices is that they can be utilised actively during flight, to optimise the spanwise lift distribution (Rivero et al., 2018), which is very important, for example, for the control of the roll movement of the aircraft.

It is also of relevant interest that this kind of technology has the potential to significantly reduce the environmental impact of the aviation sector, by reducing fuel consumption (Burdette & Martins, 2019; Greff, 1990). This fuel reduction is accomplished due to the fact that these devices achieve lift coefficients with less drag involved, leading to less energy needed and so less fuel to maintain the thrust required during the multiple flight stages.

As a result of the aspects explained above, there has been considerable interest in recent years in implementing this type of mechanism. This is partly due to the environmental impact and efficiency needs, but also due to developments in smart materials and composite structures (Rivero et al., 2018). This progresses contributed to the process of overcoming the main issues, that the initial variable camber concepts had: heavy and complex mechanisms that reduced their overall benefit (Rivero et al., 2018).

Barbarino, Bilgen, Ajaj, Friswell, and Inman (2011) and Thill, Etches, Bond, Potter, and Weaver (2008) and Valasek (2012) have summarised some research on morphing wings and emphasised that dynamic changes in the camber distribution of aerofoils are one of the most often studied and explored approaches, with the objective of maximising aerodynamic performance (Rivero et al., 2018).

2.2.1 Historical Overview

The NASA F-111 Mission Adaptive Wing aircraft (MAW), presented by Larson (1986), Figure 2.2, featured one of the earliest designs, that attempted adjustable camber without surface discontinuities, with no spoilers, external flap hinges, or fairings to break the smooth contour of the wing. This MAW was a variable camber wing with flexible leading and trailing edge flaps that has the purpose of maximising aerodynamic performance, under various flight conditions.

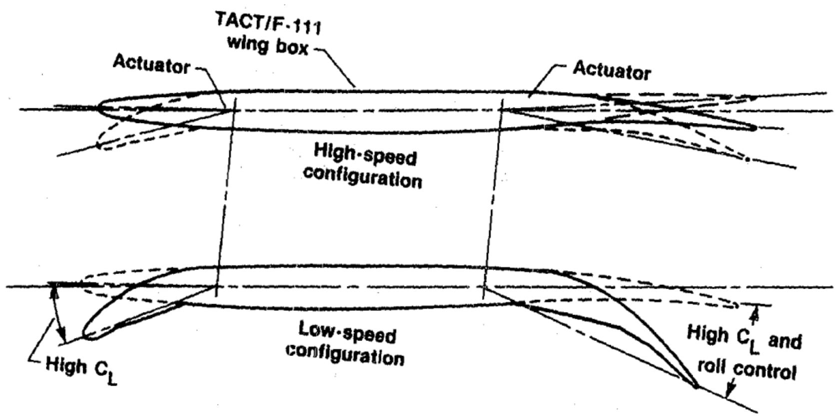

Figure 2.2: Variable camber movement of the NASA F-111 MAW (adapted from Larson (1986)).

The DARPA Smart Wing developed by Kudva (2004), Figure 2.3 is another proposal for variable camber, it uses a centre laminate with a honeycomb core and high strain-to-failure silicone skin to provide the trailing edge elasticity needed to produce camber variations (Rivero et al., 2018).

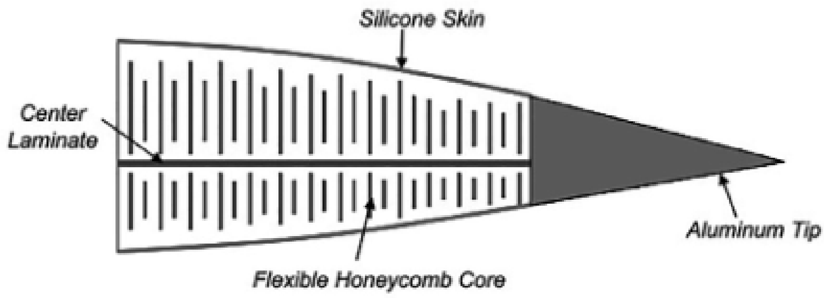

Figure 2.3: DARPA smart wing variable camber concept (adapted from Kudva (2004)).

Also, devices placed on the leading edge have been used by several research teams to study the variation in camber. Vasista et al. (2017), for example, developed and produced a compliant ”droop-nose” morphing leading-edge device employing super-elastic materials (Rivero et al., 2018).

Further, the feasibility of combining leading and trailing edge morphing devices within the same wing has been studied. Kota et al. (2003) conducted a study on this topic using voice coil motors and piezoelectric actuators, and Gaspari, Ricci, and Riccobene (2014) designed, produced, and tested a variable camber wing with morphing leading and trailing edge devices based on compliant-based mechanisms (Rivero et al., 2018).

Additionally, Monner, Kintscher, Lorkowski, and Storm (2009) suggested a composite monolithic compliant morphing trailing edge device, although, no actuation device was chosen. It is also relevant to mention that Gaspari and Ricci (2010) also carried out a two-level optimization that first delivered the ”best” aerofoil design for a certain situation, before delivering the best internal structural configuration capable of producing that aerofoil geometry (Rivero et al., 2018).

Moreover, some models achieved dynamic camber by placing the camber changes on the trailing edge. Bilgen, Friswell, Kochersberger, and Inman (2011) presented a concept that employed two integrated active bimorph actuators, which form the top and bottom trailing surfaces of the aerofoil skin. The actuators used in this model were the Macro-Fiber Composite (MFC) actuators, that is a layered, planar actuation device that employs rectangular cross-section, unidirectional piezoceramic fibers embedded in a thermosetting polymer matrix.

In this same idea, Molinari et al. (2011) suggested an actuator system on the trailing edge based on the ”smart material” called Dielectric Elastomer (DE). This type of material is able to deform when subjected to an electric field, bringing the possibility of exploiting their sensing capabilities and enabling the creation of a control system based on sensors, without requiring any extra structural components.

One other model of a camber morphing device was developed by Daynes et al. (2010), applied to a flap in a rotor blade section. This flap was based on the bistability that non-symmetric fiber-reinforced composite laminates present. This inherent bistability applied to the flap showed the potential of an energy-efficient design because the actuator used only required to do work when moving between the two stable positions defined, not to hold these positions continuously.

Barbarino et al. (2009) also proposed a morphing wing trailing edge concept which included a compliant rib structure that made use of Shape Memory Alloys (SMA) actuators, Figure 2.4. The concept was constituted by five shaped panels, connected in couples by crossed laminas, working as spring elements and the SMA elements, with a wire shape, were located under the springs. When their activation occurred, there is a contract of these elements that leads to a rotation of the rib parts having a direct consequence in the camber variations.

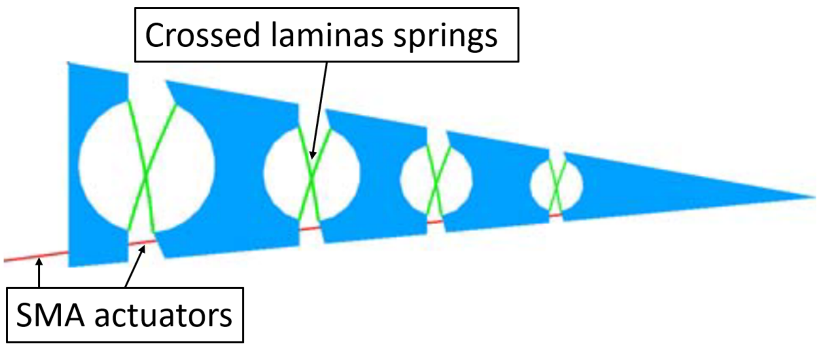

Figure 2.4: Rib architecture of the SMA-based concept for a camber morphing wing (adapted from Barbarino et al. (2009)).

As Milojević and Pavlović (2016) mentions, the current design process of morphing compliant structures frequently results in systems with intersecting structural parts and actuators, which are particularly challenging to fabricate. Therefore, Milojević and Pavlović presented an enhanced design methodology since it proposes compliant systems without overlapping elements. They also developed and produced an adaptive shape morphing compliant structure with embedded actuators that was obtained through an optimisation process.

A promising morphing wing concept that made use of active actuation of the internal load-bearing structural members for the movement of the trailing edge was presented by Previtali et al. (2016). Their work showed a compliant wing concept that featured a load-carrying, doubly corrugated morphing skin, which allowed the structure to be flexible and efficient. This structure is represented in Figure 2.5 where the skin is depicted in blue colour, the rib in red, the spar in green, the corrugation in magenta and the actuator in black.

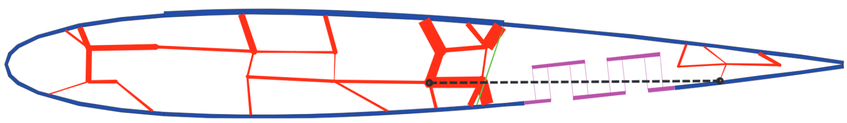

Figure 2.5: Morphing wing representation with an enhanced corrugated skin (adapted from Previtali et al. (2016)).

2.3 Fish Bone Active Camber (FishBAC)

The FishBAC, developed by Woods and Friswell (2012), is one idea that has shown potential to be further studied due to the promising aerodynamic results and the developments that have been presented in the terms of manufacturability (Rivero et al., 2022).

As Rivero et al. (2022) defined, this compliance-based morphing aerofoil (Figure 2.6) inspired by the fish anatomy, is made of a skin covering an internal skeleton system. The skin is constructed of pre-tensioned Elastomeric Matrix Composite (EMC) materials and is supported by several spanwise stringers that branch off from a central bending beam spine. This spine is made of a thin composite plate placed in the centre of the aerofoil (Rivero et al., 2022). To achieve the shape change needed for operation, a series of tendon spooling actuation mechanisms are placed along the span. In this actuation mechanism, when a specific torque (T) is applied to the pulleys, the tendons get tensioned and transmit this rotational force to the trailing edge, where the tendons are fixed, making the aerofoil change its camber (Rivero et al., 2022)).

2.3.1 Historical Overview

Since FishBAC was presented for the first time in 2012, some modifications in the manufacturing process and in the material selection have occurred, and new versions of this model have appeared.

As Rivero et al. (2022) considered, the first generation of FishBAC devices (Figure 2.7) had 3D printing as the main form of manufacturing. This version had a single internal "skeleton", constituted by the stringers and the spine, that was printed in one single piece made of Acrylonitrile Butadiene Styrene (ABS) plastic. Then, a silicone elastomer skin was further pre-stretched and glued to this skeleton, while

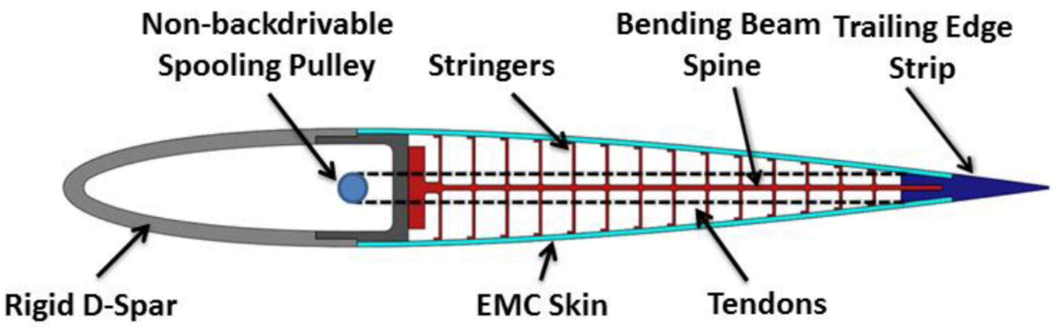

Figure 2.6: Aerofoil view of the Fish Bone Active Camber concept (Woods & Friswell, 2013).

the pulley mechanisms were produced separately and added subsequently. The actuation loads were transferred from the servos to the trailing edge of the morphing device using Kevlar tendons. These were hand-stitched to the trailing edge on one end and connected to the pulleys on the other (Woods & Friswell, 2013 and Woods & Friswell, 2014).

Figure 2.7: First generation of the FishBAC (Woods & Friswell, 2014).

A key aspect of this design is related to the fact that, by using the 3D Printing technology, the stringers did not need to be later attached to the spine and the number of parts could be reduced. However, 3D-printed ABS plastic is far from an ideal material to be used in the aeronautical area due to its stiffness and strength. Despite that, this generation has shown to be crucial to the study of the aerodynamic advantages of the FishBAC concept with this model being thoroughly experimented with in a wind tunnel (Woods & Friswell, 2013).

Following the classification made by Rivero et al. (2022), Figure 2.8 shows the second generation of FishBAC devices, that was designed with the main objective to include carbon fiber-reinforced composite into the spine. This material has much better structural qualities than 3D-printed plastics, and it also enables this structural part to have the desired stiffness according to the differences in fibre angle in each ply of the composite (Rivero et al., 2018).

As was also the case for the first generation, this second one demonstrated the obvious aerodynamic advantages that this camber morphing mechanism has, when compared to a conventional hinged trailing-edge flap of similar dimensions (Rivero, Fournier, Manolesos, Cooper, & Woods, 2021). This is more noticeable at high lift coefficients where the improvements of lift over drag ratio are above 250%

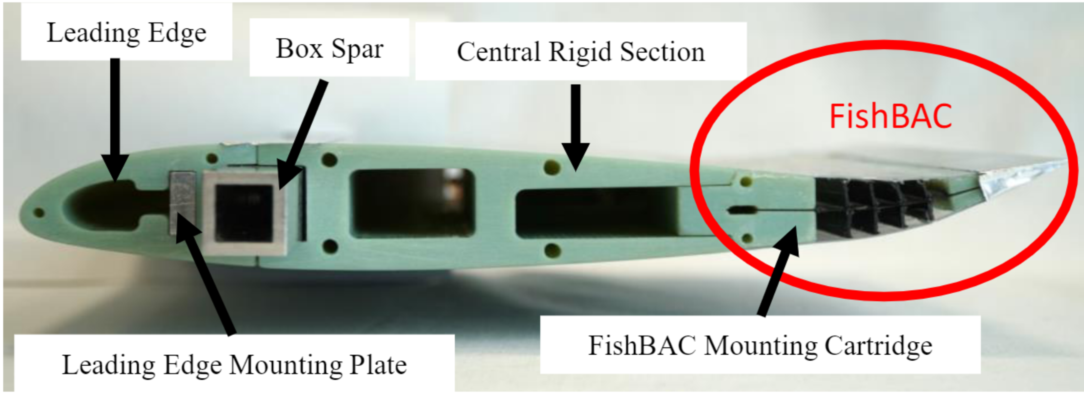

Figure 2.8: Second generation of the FishBAC (Rivero et al., 2018).

and for $C_L \approx 0.5$ the minimum efficiency improvement is of 16% (Rivero et al., 2020). This fact is supported by the wind tunnel data represented in Figure 2.9. It is important to mention that the baseline in the Figure 2.9 represents the 3D printed rigid NACA 23012 trailing edge section.

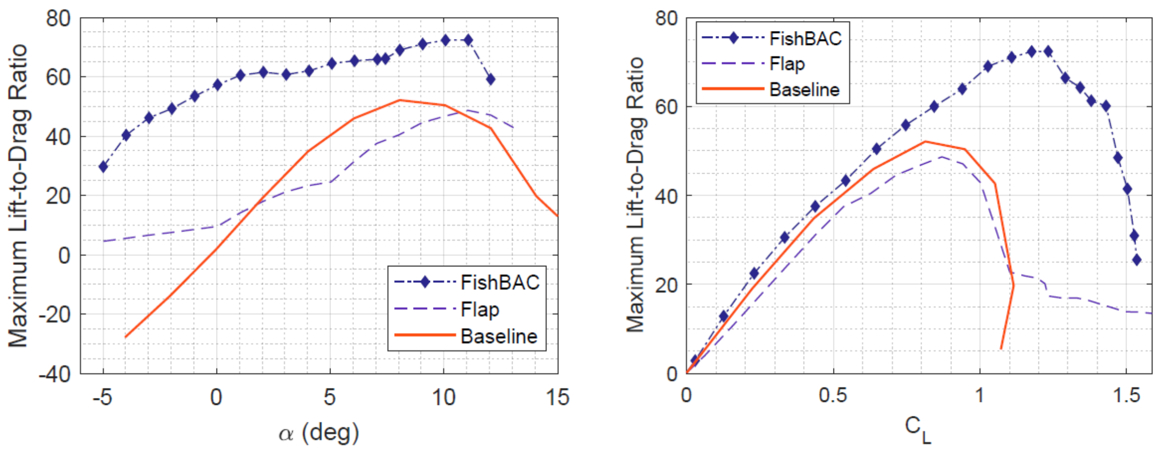

Figure 2.9: Efficiency envelopes showing the best achievable lift-to-drag ratios as a function of angle of attack (left) and of lift coefficient (right) (Rivero et al., 2020).

Finally, a third generation was introduced by Rivero et al. (2022). A representation of this design is shown in Figure 2.10.

The main objectives of this design, as Rivero et al. (2022) mentioned, were to tackle the limitations of the first and second generations by achieving three principal requirements. The first requirement was to facilitate the removal and repair processes for any structural part. The second one, was to allow the adjustment of the tension applied to the tendons and, the last one, was to have the skins and stringers attached without using any adhesive (Rivero et al., 2022). To make this design possible, and to be able to meet the above criteria, the actuation mechanisms were produced using machining, the spine was manufactured using composite hand layup and the new morphing skin design was produced by using multi-material Fused Filament Fabrication (FFF) (Rivero et al., 2022). This process, as Rivero et al. (2021) defined, produced the skins and the stringers together, using two different materials that

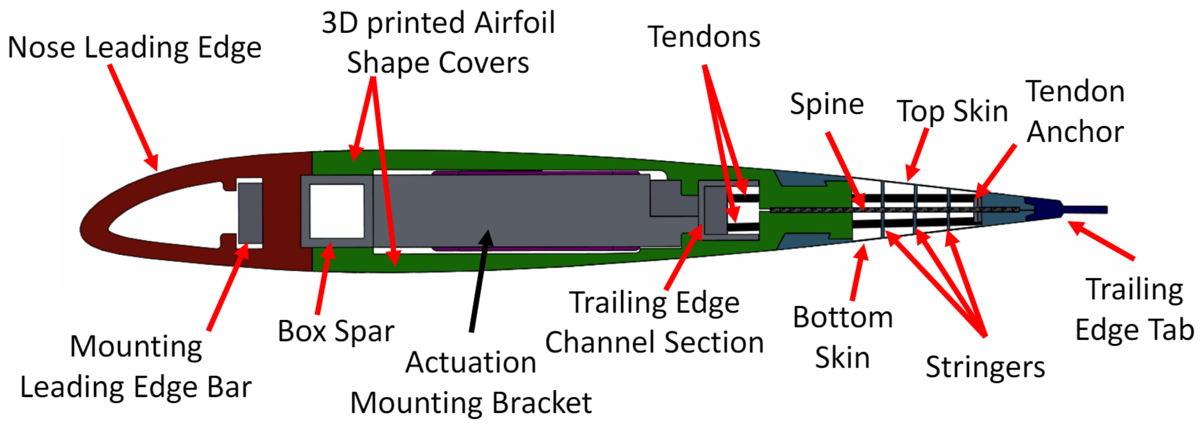

Figure 2.10: Representation of the third generation of the FishBAC in the chordwise direction (Rivero et al., 2022).

were fused during the printing process. The skin was produced using the Ninjatek Ninjaflex Thermoplastic polyurethane (TPU) and the material selected to build the stringers was the Ninjatek Armadillo TPU. These 3D printed Geometrically Anisotropic Thermoplastic Rubber (GATOR) morphing skins are discussed further in Heeb, Dicker, and Woods (2022).

It is important to mention, that the wingspan that was used in the study of this third generation was a 995 mm ($b = 995$ mm) and the aerofoil used was the NACA 23012, modified with a trailing-edge tab and having a 270 mm chord length ($c = 270$ mm). This aerofoil was selected to match the one used in the Bo-105 helicopter, which is the baseline rotor system of the EU Horizon 2020's *Shape Adaptive Blades for Rotorcraft Efficiency* (2021) SABRE project, for which the work from Rivero et al. (2022) was carried out. The actual camber morphing device is located in the rear 25% of the airfoil section, i.e., beginning at $x/c = 0.75$, making the front 75% of the airfoil section rigid. In terms of stiffness and actuation requirements, this third generation used, as baseline, the same conditions described by Rivero et al. (2018) for the second generation FishBAC.

In order to achieve the camber that the device is intended to do, actuations systems are mounted. This actuation occurs at three discrete points spaced along the trailing edge, as it can be seen in Figure 2.11

As Rivero et al. (2022) pointed out, an important limitation of the second generation design was the significant amount of elastic washout observed along the spanwise direction. This elastic washout happens when the wing presents different values of deflection of the trailing edge for a given actuation load that is the same in all actuation points. In response to this phenomenon, Rivero et al. (2022) added an extra actuation point at the midpoint of the wing span (Figure 2.11) and performed a study in order to select the best composite configuration for the spine, with special attention to the number of plies and stacking sequence. The selected one was the [90/90/0/90/90] with five plies of 8552/IM7 Unidirectional (UD) carbon fiber prepreg with a total thickness of 0.65 mm, as it showed to have the ability to achieve the largest deflections (w_{max}) under a specific actuation load and, the lowest variation in transverse displacement along the span (w_{min}/w_{max}), within the range of stacking sequences that were studied by

Rivero et al. (2022).

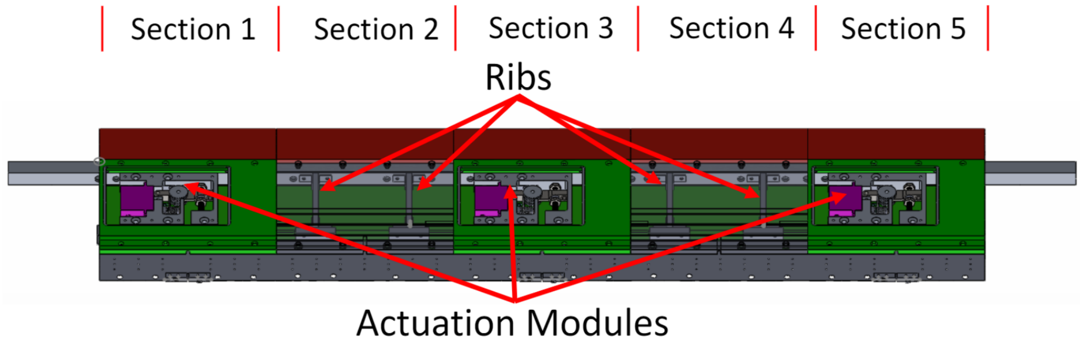

Figure 2.11: Representation of the third generation of the FishBAC in the spanwise direction (Rivero et al., 2022).

It is important to mention that Rivero et al. (2022), in order to obtain the properties of the materials used in the design, three tests were performed: a carbon fibre axial, transverse and shear tensile tests, and Armadillo TPU (stringers) and Ninjaflex TPU (skin) tensile tests. From these tests Rivero et al. (2022) obtained the stress–strain curves that make possible the determination of the fibre-direction (E_{11}), matrix-direction (E_{22}) and shear (G_{12}) modulus for the carbon fiber-reinforced polymer (CFRP). Additionally, the in-plane Poisson's ratio (ν_{12}) was obtained from both (E_{11}) and (E_{22}) while (ν_{23}) was obtained from a typical assumption for CFRP UD laminates, where $G_{23} = E_{22}/2(1+\nu_{23})$ (Çınar, Ozturk, Ersoy, & Wisnom, 2014). Due to the fact that Ninjaflex TPU and Armadillo TPU materials are isotropic materials, E and ν were obtained from the experimental data and G using the expression for this type of materials $G = E/2(1+\nu)$. Table 2.1 shows all the material properties obtained from the experimental results obtained by Rivero et al. (2022).

Table 2.1: Summary of material properties of the third generation of the FishBAC (Rivero et al., 2022).

Material	8552/IM7	Armadillo	Ninjaflex
E_{11}	168.91 GPa		
E_{22}	8.00 GPa	275 MPa	15.3 MPa
E_{33}	8.00 GPa		
G_{12}	4.79 GPa		
G_{13}	4.79 GPa	97.0 MPa	5.50 MPa
G_{23}	2.76 GPa		
ν_{12}	0.32		
ν_{13}	0.32	0.42	0.39
ν_{23}	0.45		

2.3.2 Structural considerations of a FishBAC concept

When designing a FishBAC structure that achieves a smooth camber morphing without using excessive amounts of mechanical complexity, it is necessary to consider employing materials and a specific geometry that are able to produce a structure capable of bending along the chord to alter camber, but also add anisotropic reinforcement to preserve stiffness in the other loading directions (Rivero et al., 2018). The addition of spanwise rigidity is important to achieve uniform spanwise shapes, avoiding the elastic washout, but it can influence the stiffness in the direction of shape change (Rivero et al., 2022), making this a critical balance that needs to be taken into consideration, when designing this type of camber morphing mechanism.

As a result, all design concepts typically contain a variety of structural components and material kinds that are joined in specific ways. Making these multi-element and multi-material devices is, therefore, one of the primary challenges in camber morphing research (Rivero et al., 2022).

Chapter 3

Implementation

3.1 Problem Description

The three models that have been presented in Chapter 2.3.1 have shown some limitations. All three generations have shown one common issue, the elastic washout. This is clearly a problem that needs to be addressed. Conceiving a innovative and efficient solution for this issue can be challenging. There are factors that have to be considered on all aeronautical structures: they must be as lightweight as possible, easy to maintain, have a reduced impact on the environment and, of course, with the lowest cost possible involved.

3.2 Solutions to study

Having a better understanding of the FishBAC behaviour is crucial. Its constitutive parts, the respective functions and typical materials used as well as its problems and limitations, will make it now possible to start the process of generating new ideas, that might turn into viable solutions.

This process of brainstorming ideas and solutions was done considering the third generation of the FishBAC presented by Rivero et al. (2022). For every main component, a different uppercase letter was designated: A - spine; B - stringers; C - skins; D - trailing edge and E - actuation points. At least one idea was found for every component.

The ideas considered were:

- A1 - Cutouts in the spine plate;
- B1 - CFRP pultrusions added to the stringer and next to the skin;
- B2 - Multi-stiffness TPU stringers with ”compliant hinges”;
- B3 - Stringer cutouts;
- C1 - Spanwise reinforcement with stiffeners of TPU/CFRP reinforcement
- D1 - CFRP reinforcement with embedded pultrusions

• E1 - More actuation points with specific actuation loads.

The idea A1, consists of removing a certain percentage of material from the spine in both chord and spanwise directions. This idea has the purpose of diminishing the overall weight and giving less stiffness to the spine.

The intention of the B1 idea is to better distribute the deformation of the stringer along the span, especially, as far as possible from the spine. This is accomplished by creating some attachments that can make room for the CFRP pultrusions to be inserted between the stringer and the skin.

The solution called B2 has as a principle the usage of different stringer that has two different materials with different rigidity. These are 3D printed so that a grid is formed by the material that is more rigid and the junctions of the grid are made by the less rigid material, forming the so-called ”compliant hinges”.

The basis of the case of model B3, as mentioned for idea A1, is to remove a certain percentage of material but, in this case, for the stringer.

The solution defined as C1 is based on the incorporation of structural reinforcements made of CFRP or TPU, along the spanwise duration, placed next to the skin.

The idea D1 is similar to the idea B1 but, in this case, the CFRP pultrusions were placed on the trailing edge of the device.

Finally, solution model E1, consists in adding more actuation points throughout the wing span. In these added actuation stations, an increase in the T must be applied in a certain way so that the deflections of the tailing edge would be more similar, attenuating the elastic washout effect.

3.2.1 Decision process

Having listed the ideas and comprehending their structure, materials and production process involved, a decision process was conducted to help filter out the most relevant and promising design ideas, considering the main objectives of this dissertation. The decision process used was the Analytic Hierarchy Process (AHP). This process is based on the identification of alternative solutions for the problem to be solved and the criteria to access the options of possible solutions. Then these criteria are quantified according to the objectives of the study and the solutions ideas are evaluated and converted into a numeric value within each criteria. Then both these values attributed to the criteria and the alternative options are used to calculate a number that represents the most desired solution.

The decision process executed began with a selection of different criteria. The defined criteria were elaborated in order to better suit the final objectives of the work being currently developed, tackling the limitations of the FishBAC. Due to the fact that the different defined criteria have different importance weights in the achievement of the objectives of this study, a system of ratings was considered. These ratings were defined in a scale from 1 to 5, with the value 1 representing less important criteria and 5 the most important. The defined criteria and respective ratings are presented in Table 3.1.

In the next step of the decision process, the ideas were classified within each criteria. This process assesses the capacity of an idea to achieve what is stated by the criteria and it is shown in the decision matrix presented in Table 3.2. The classification also uses a scale from 1 to 5, where 1 is given to an idea

Table 3.1: Decision criteria used in the assessment of the ideas.

Criteria#	**Criteria**	**Criteria rating**
1	Effectiveness to reduce washout	5
2	Torsional rigidity	4
3	Capability to achieve large spanwise deformation	4
4	Risk to achieve the objectives	4
5	Complexity of the build	3
6	Cost of the build	3
7	Easier Maintenace of the concept	2

that can not fulfil the objective define in a certain criteria and 5 to the idea that can easily accomplish it. It is important to mention that this assessment was done using a personal engineering judgement of the importance of each criteria and idea, resulting in qualitative assessments being turned into a quantitative decision process.

Subsequently, the criteria ratings were multiplied by the idea rating, resulting in the values that are presented in weighted rating rows of Table 3.2. In the column situated furthest to the right, is presented the summation of all weighted ratings of each idea model. This value indicates, in a quantitative way, how a model can deliver a result that can respond to the objectives. Considering this, the models selected to be further investigated were the A1 and B1 because of their high scores values.

Table 3.2: Decision matrix using the defined criteria and ratings.

Criteria #	1	2	3	4	5	6	7	Total
Criteria rating	5	4	4	4	3	3	2	125
Idea A.1	3	4	4	3	4	4	3	
Weighted rating	15	16	16	12	12	12	6	89
Idea B.1	4	3	3	4	3	3	4	
Weighted rating	20	12	12	16	9	9	8	86
Idea B.2	3	4	4	3	3	3	3	
Weighted rating	15	16	16	12	9	9	6	83
Idea B.3	3	4	4	3	3	3	3	
Weighted rating	15	16	16	12	9	9	6	83
Idea C.1	4	3	3	4	3	3	3	
Weighted rating	20	12	12	16	9	9	6	84
Idea D.1	4	3	3	4	3	3	3	
Weighted rating	20	12	12	16	9	9	6	84
Idea E.1	4	4	4	4	2	2	2	
Weighted rating	20	16	16	16	6	6	4	84

3.3 Baseline Model

In order to understand the effect of the ideas that were decided to be investigated, a baseline model was designed and will be used as a reference to compare the solutions proposed in this work. This model was designed using, as a reference, the third generation of FishBAC designs presented in Chapter 2.3.1. It is a simplified version that includes all major components, namely the skin, spine, stringers and a rigid trailing edge part.

It is essential to mention, that this model only represents the section of the wing where the camber morphing part is localised, which starts at 75% of the aerofoil chord. The aerofoil, chord dimensions and span used were the same as the ones used in the third generation of FishBAC designs, presented in Chapter 2.3.1.

3.3.1 CAD model

Siemens NX was the computational program chosen, not only to elaborate the CAD for the baseline model but also to perform the FEA. This software has the Simcenter Nastran 2020 program responsible for the Finite Element Method (FEM) which was used in version 1911. This choice of software was based on the knowledge previously acquired in working with this program.

Firstly, the aerofoil was sketched in 2D, using the reference points delivered by the database in Airfoil Tools (2022). From this, two vertical lines were drawn, one where the morphing part begins ($x/c = 0.75$) and the other line closer to the leading edge (for $x/c \approx 0.65$). These lines, in addition to the lines that define the 2D aerofoil form the plane that will be later extruded to form the rigid part closest to the leading edge of the wing. In a similar process, another vertical line was drawn at $x/c = 0.9$, defining the limit of the plane that will later generate the trailing edge rigid part. Both, linked with rigid parts, are depicted in Figure 3.1 with a green colour. Subsequently, a horizontal line, placed in the middle of the aerofoil is defined, beginning at $x/c = 0.75$ and ending at $x/c = 0.9$. This line will later be used to establish the spine of the model. Still, inside the mentioned range ($x/c = 0.75$ and $x/c = 0.9$), three other vertical lines were perfectly distributed, being equally spaced between them and between the limits of the morphing section. These lines were created in order to define the stringer of this design. This complete 2D sketch, seen in Figure 3.1, presents the final profile that is extruded in the normal direction of the plane where it was drawn, forming the 3D CAD. This extrusion was done until the 3D structure had a wingspan of 995 mm, equal to the one mentioned in Chapter 2.3.1.

The final CAD is presented in Figure 3.2, using the green colour for the representation of the rigid parts, pink colour for the skin, dark blue for the stringers and red for the spine.

3.3.2 Finite Element Analysis

3.3.2.1 Mesh, Element types and Material properties

Following the FEA steps mentioned in Chapter 2.1.2, after having the CAD file created, it is necessary to assign a specific mesh to the geometric model.

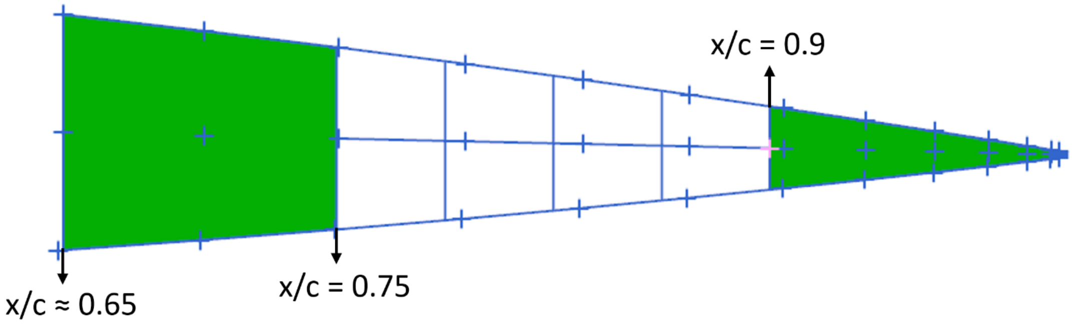

Figure 3.1: Final 2D sketch for the baseline model CAD.

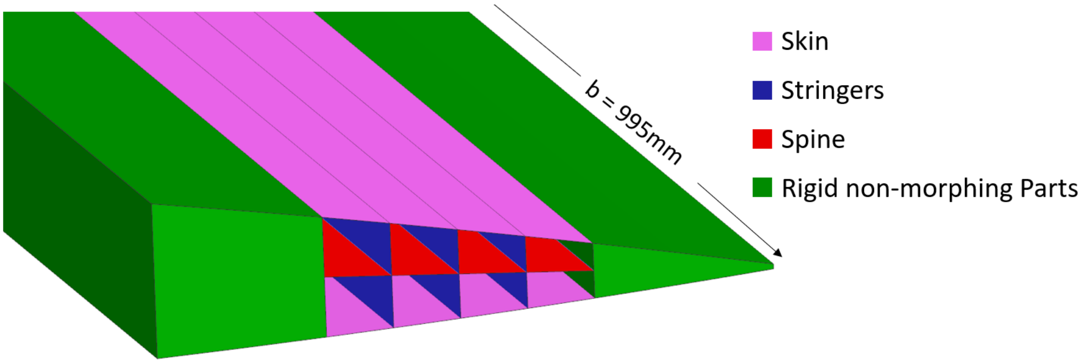

Figure 3.2: Isometric perspective of a portion of the baseline model CAD.

Siemens NX has the capability of generating an automatic mesh taking into consideration the relationship between the total volume of the component and the surface area, among other geometric characteristics. For a modelled component (surface or solid), it is possible to prescribe to the software the desired finite element geometry and the base size of the element, for which the initial value used in this work was 3 mm for all elements generated.

In this case, for the 2D surfaces that represent the skin and the stringers, quadrilateral shell elements were used, due to the fact that these types of elements are able to resist bending loads and they are ideal for modelling thin plates. These elements are designated as PSHELL in the Siemens NX software. In terms of the shape of the elements, the CQUAD4 (quadrilateral element with four nodes) was used for the skin, stringers and spine because all these components of the FishBAC have a rectangular-like configuration. In the software of Siemens NX, the CQUAD4 elements are based on the Mindlin-Reissner shell theory. These elements do not provide direct elastic stiffness for the rotational degrees of freedom which are normal to the surface of the element.

The CHEXA(8) element, as it is defined in the Siemens NX software, is a six-sided solid element (PSOLID) that was selected to represent the more rigid and 3D portions of the model, due to the need to capture the complexity of the geometry and the possibility of three-dimensional deformations.

It is also important to mention that, all these elements used are linear and the simulations being developed are Linear Statics FEA. Due to this, it is possible to say that, the greater the number of elements involved, the more refined the mesh will be and better precision in the results is obtained. It is also important to mention that the number of nodes is directly related to the degrees of freedom of the element, which influences the accuracy but also increases the computation time. A convergence study will be presented later to support the choice of mesh.

The obtained mesh is represented in Figure 3.3, where the green elements are the CQUAD4 and the orange ones are CHEXA(8).

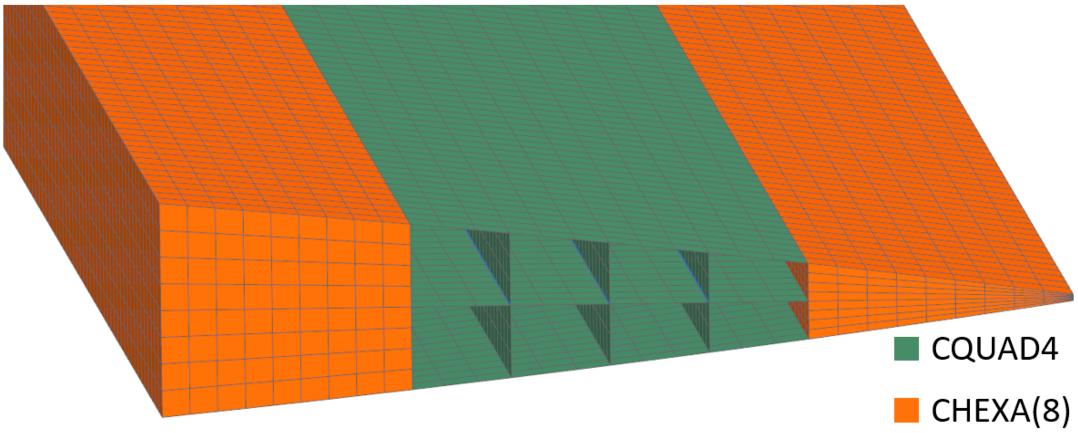

Figure 3.3: Mesh used with CQUAD4 and CHEXA(8) elements.

The material assigned to the mesh of the rigid non-morphing parts was aluminium 2014-O, whose properties were introduced in the software. The values used were taken from the database in MatWeb (2022) and are shown in Table 3.3.

For the rest of the components, the materials used for the 2D meshes were the exact same used in the third generation design of the FishBAC.

All properties used in the model are listed in Table 3.3.

Siemens NX has the great advantage of making it possible to simulate and analyse the behaviour of composite materials. This is relevant for the study since one of the main components, the spine, is made of a laminated composite material.

The first step for the simulation of composites is the introduction of the properties of the materials in use. The software allows to list the properties of various types of materials such as uni-directional laminates, orthotropic materials and isotropic materials. In this case, the properties of the 8552/IM7 material used in the laminate have been defined and presented in Table 3.3. It is worth to refer that these properties are referring to the entire composite, i.e., fibres with the respective matrix.

Next, we define the type of material we want to assign to each mesh. In other words, it is possible to indicate to the program the type of component to use: 3D, 2D shell, laminate, among others. In this case, the objective is to use the laminate type.

Finally, it is necessary to give the program information about the configuration, thickness and material of the laminates. This is done by inserting the stacking sequence and manually creating the plies. It is also possible to enter this information using the shorthand format. For this case, this last option was used using the same format as the third generation of FishBAC [90/90/0/90/90] with a thickness of 0.13 mm for each ply, making a total of 0.65 mm for the spine panel.

Table 3.3: Summary of material properties of the third generation of the FishBAC (Rivero et al., 2022).

Material	8552/IM7	Armadillo	Ninjaflex	Aluminum 2014-O
E_{11}	168.91 GPa			
E_{22}	8.00 GPa	275 MPa	15.3 MPa	72.4 GPa
E_{33}	8.00 GPa			
G_{12}	4.79 GPa			
G_{13}	4.79 GPa	97.0 MPa	5.50 MPa	28.0 GPa
G_{23}	2.76 GPa			
ν_{12}	0.32			
ν_{13}	0.32	0.42	0.39	0.33
ν_{23}	0.45			

3.3.2.2 Boundary conditions and Applied loads

In order to perform the simulations related to the structural analysis it is necessary to define the boundary conditions to be applied to the model. The only constraint that needs to be applied to the model, for the FEA being developed, is to fix all the degrees of freedom of the rigid part that is closer to the leading edge of the wing, marked in with orange colour in Figure 3.4. This prevents translation and rotation movements in any direction.

Regarding the loads applied, T is applied to the spine, in the nodes that are closest to the three locations where the tendons anchors were connected to the spine, considering the third generation model FishBAC presented by Rivero et al. (2022). The value used was 4 Nm applied in the direction that makes the trailing edge deflect downwards, in the negative direction of the global y-axis, as seen in Figure 3.4. It is also important to mention that this value of 4 Nm was used as it gave useful levels of deflection while still being in the range of what is achievable from commercially available servo actuators.

Lastly, it is important to mention that Glue Connections were used to ensure that the 2D Laminate elements were secured to the 3D solid elements. This type of function of the software creates a rigid connection between surfaces and/or edges of a specific surface and is a way of maintaining the position of the different meshes created, in cases where the elements are of different dimensions (2D and 3D). The rest of the elements were connected using the Sew function of Siemens NX. This command is used to combine thin 2D bodies by sewing common edges together or common faces and this is done before creating the mesh. This guarantees that when creating the mesh for the different 2D bodies, the mesh is connected as pretended. By using this method, the connection process was much easier and more robust to the possible modifications that are needed in further analysis.

3.3.2.3 Verification and Validation

Having gone through all the previous steps of the FEA, it was time to run the simulation and verify the solution.

Figure 3.5 presents the values of deflection of the trailing edge, in the negative direction of the global y-axis, along the spanwise direction. It is possible to clearly see three vertices in the location where the

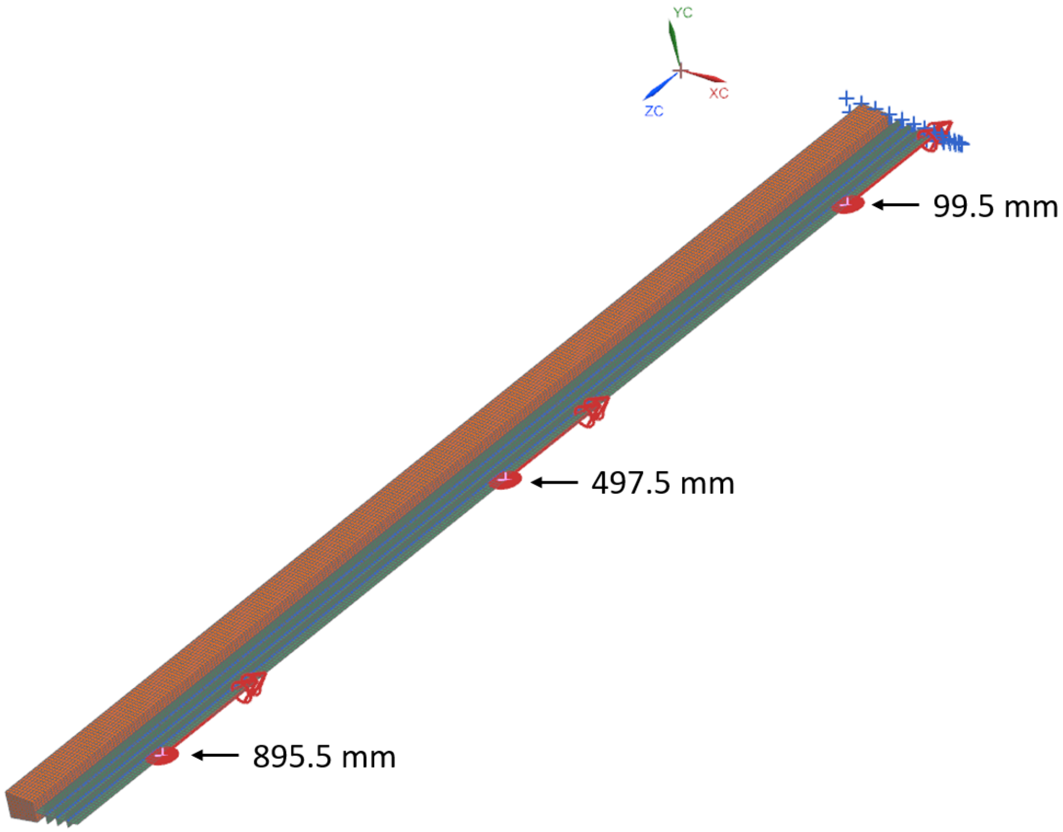

Figure 3.4: Mesh, applied Load and constrains.

torques were applied. This corresponds to the location of the actuators that have as coordinates 99.5 mm, 497.5 mm and 895.5 mm in the spanwise direction.

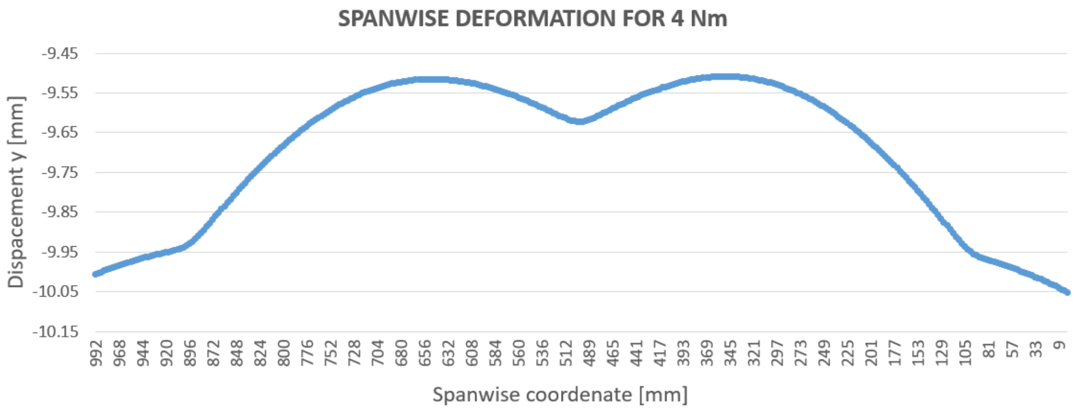

Figure 3.5: Spanwise deformation of the trailing edge for a T of 4 Nm.

The displacement of the trailing edge at the span midpoint was 9.62 mm. This level of deflection is reasonable as it allows for significant variation of the lift coefficient (C_L) with a modest impact on drag, which is the intention for this type of morphing device. As referred by Woods, Fincham, and Friswell (2014), the value of deformation for a morphing device like this must be up to 10% of the total chord of the aerofoil. In this case, the value obtained is close to 3.5% of the total chord of 270 mm, witch is acceptable for the value of torque applied in this phase of the study.

The shape of the spanwise deformation is not perfectly symmetric as it can be seen in Figure 3.5. This is acceptable because the order of magnitude of the difference in the values of the deformation, considering two symmetric locations, is about 10^{-2} mm.

While the exact cause of the asymmetry in the response is not known for certain, it is likely due to either inconsistency in the mesh or perhaps some other form of numerical inconsistency. While not ideal, the overall deformation values are much higher than the asymmetries in the deformation, and the spanwise variation is also significantly larger than the asymmetry, allowing the possibility to meaningfully consider the impact of design changes on the overall deformation and its spanwise variation, despite the asymmetry.

It is also important to mention that the stress registered in all components of the structure was below the limit of stress for the linear elastic behaviour (yield strength) of the materials used for each component.

3.3.3 Mesh Convergence Test

As mentioned in Chapter 3.3.2.1, for Linear Statics FEA using linear elements, the number of elements used relates to the accuracy of the solution results and the computing time needed to obtain them. Consequently, it is necessary to perform a mesh convergence study, to ascertain the best compromise between the number of elements and computation cost. In critical areas, it is advisable to use a more refined mesh compared to the rest of the components, to obtain a more efficient and accurate simulation (Niu, 1999).

As mentioned in Chapter 3.3.2.1, the initial element base size was 3 mm and the results were validated as described in Chapter 3.3.2.3.

From this, the element base size was reduced in half (1.5 mm) for all the components with the different types of elements (2D shell, 2D Laminate and 3D solid), keeping their relative size similar and their geometry constant, in order to obtain consistent results between the various simulations. Similar processes were made but to obtain less refined meshes with twice (6 mm) and triple (9 mm) the base size of the initial 3 mm value considered. It is also important to mention the number of elements for each mesh. The 9 mm mesh presented a total of 4662 elements, the 6 mm mesh had 16932 elements, the 3 mm mesh had 64408 and finally, the 1.5 mm mesh contained a total of 257244 elements.

To better analyse the convergence of the meshes obtained, a plot was elaborated relating the displacement at the span midpoint, the number of elements and the computing time. This plot is presented in figure 3.6.

It was possible to verify that, the simulation runtime for 1.5 mm was more than four times bigger than the computing time obtain for the 3 mm mesh. For the 6 mm simulation, the computational time was more than three times quicker than the time obtain for the 3 mm mesh and for the 9 mm mesh, more than six times.

Finally, as the last step of a convergence test, a criteria must be defined, in other to know if there is an effective convergence and stop the mesh refining. This is usually called the stopping criteria. In this case, the stopping criteria is defined using the absolute relative difference of the displacement values at

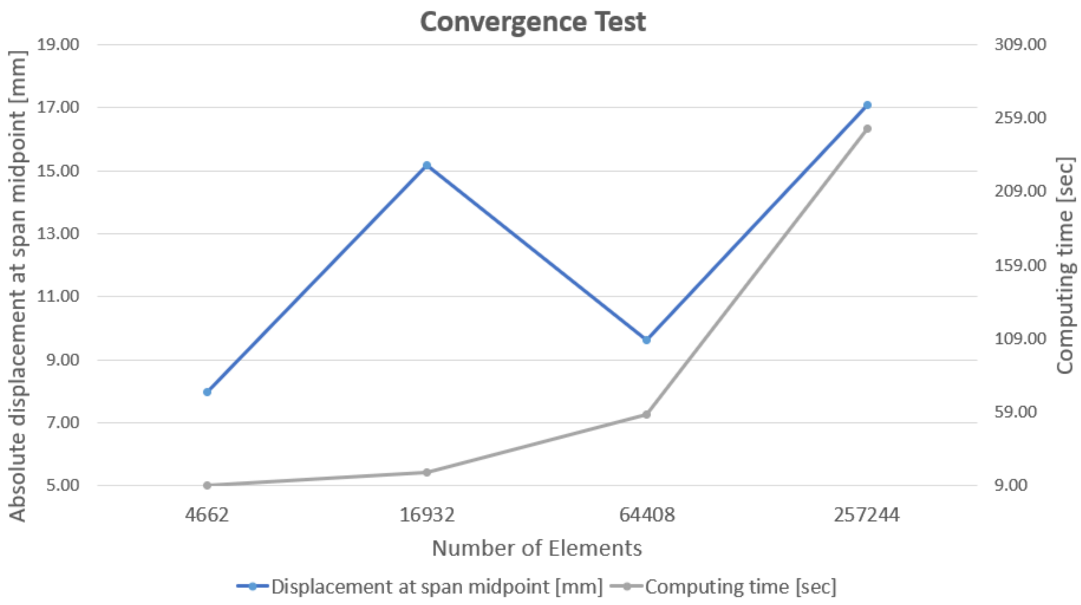

Figure 3.6: Mesh convergence test.

the span midpoint. If that absolute relative difference is less the 5%, it can be considered that the mesh has converged and continuing the refinement process will not give a much different result compared to the present one.

In this mesh converging test, the absolute relative differences have really high values when compared to the intended value of 5%, as it can be seen in Table 3.4.

Table 3.4: Mesh converging Test

Nº Elements	Computing time [seg]	$w_{s/2}$ [mm]	Absolute relative difference [%]
4662	9.01	7.97	-
16932	18.34	15.16	47.39
64408	57.67	9.62	57.51
257244	251.89	17.10	43.72

While the results of the mesh convergence study were somewhat inconclusive due to potential inconsistencies in the implementation of the different mesh sizes, the 3mm mesh was chosen as it still provided the most useful balance of resolution and solution time.

Chapter 4

Studied Models

As decided in Chapter 3.2.1, the models that are going to be discussed in this chapter are the A1 (cutouts in the spine plate) and B1 (CFRP pultrusions added to the stringer and next to the skin) individually. A third model combining the key features of the A1 and B1 models will also be presented and further discussed in this chapter.

It is also important to mention that all three models were designed having the baseline model as a starting point. The procedures described in Chapter 3.3 are also applied to the three models that are going to be analysed.

In order to evaluate the elastic washout, some parameters are defined and are relevant to mention.

The first parameter is the difference between maximum and minimum values of trailing edge displacement, normalised by the average displacement obtained. This is a dimensionless value and can be given by Equation 4.1.

$$\Delta_{norm} = \frac{|w_{max} - w_{min}|}{\bar{w}}. \tag{4.1}$$

The second parameter studied is the standard deviation (σ_P) that is applied to all registered values of trailing edge displacement along the span. This parameter is expressed in mm and can be defined by Equation 4.2.

$$\sigma_P = \sqrt{\frac{\sum(w - \bar{w})^2}{n}}. \tag{4.2}$$

The letter n represents the total number of points there is in the dataset that this is formula is applied to. In this case, n is equal to the number of mesh nodes along the trailing edge.

These parameters are quantitative measures of the amount of elastic washout as they deal with the variation of the trailing edge deflection along the wing span, considering the average value registered for the deflection.

These parameters were evaluated for the baseline model and also for the A1, B1 and a model that combines the A1 and B1 models.

To better understand the effects of the magnitude of the applied torque (T) in the models that are being studied, two extra simulations were performed using 1 Nm and 10 Nm, following the same procedure defined in chapter 3.3.2. The information obtained for the baseline model is important to draw conclusions of the A1, B1 and the combined models, as it will be used as a reference for the T sweep condition.

4.1 Model A1

The A1 model was defined starting from the baseline model and making a certain number of openings/holes in the CAD that represents the spine. These openings/holes are called cutouts and, in this case of study, they are rectangular. The specific dimensions of this feature are related to the quantity of material that is removed.

For this model, the cutouts were designed to remove only 80% of the spine in the chordwise direction. Considering the spine chordwise direction length of 40.5 mm, the length of the cutout in that direction is 32.4 mm.

The same was defined for the spanwise direction but different percentages were studied (25%, 50% and 75%). For example, figure 4.1 shows part of the spine with cutouts configuration for 50% removal of the material in the spanwise direction. The pink dotted line represents the midpoint of the spine and the symmetry axis. This means that the spine cutouts represented are exactly equal for the other side of the spine, that is not represented in the picture.

The red line is positioned parallel to the symmetry axis and passes through the location of the outer actuation point. It is important to mention that the pink dotted line passes through the location of the central actuation point. These lines are relevant because, by design, they are references to the location of the cutouts in the spanwise direction. For example, the cutout located at the left side of the red line has its centre located at 40% distance from the red line, considering the length that goes from the left side of the spine to the red line.

The other two cutouts, that are placed between the red and pink lines, have their centre located so that the distance between both is twice the distance that separates the centre of the cutout and the closest line (pink or red).

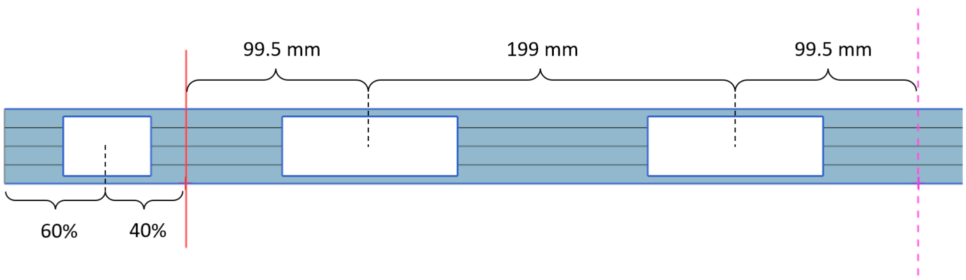

Figure 4.1: Midspan cutouts configuration with 80% of the spine removed in the chordwise direction and 50% of the spine removed in the spanwise direction.

For a better understanding of the design of the cutouts, another example is depicted in figure 4.2 where the configuration of cutouts is 80% of the spine removed in the chordwise direction and 75% of the spine removed in the spanwise direction.

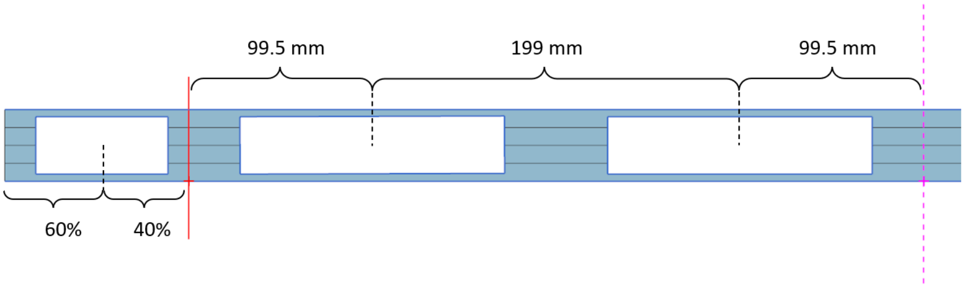

Figure 4.2: Midspan cutouts configuration with 80% of the spine removed in the chordwise direction and 75% of the spine removed in the spanwise direction.

For this new CAD, the process of generating the mesh was the same and the element base size was also maintained, as well as the one selected in Chapter 3.3.3.

4.1.1 Obtained Results

The obtained results for the spanwise displacement with relation to the different percentages of material removed are summarised in Table 4.1.

It is important to mention that the stress registered in all components of the model was below the yield strength of the materials used for each component, being the linear elastic behaviour the only one considered.

Table 4.1: Results for the spanwise displacement with relation to the different percentages of material removed.

% of material removed in spanwise direction	T [Nm]	$w_{s/2}$ [mm]	$T/w_{s/2}$ [Nm/mm]	Δ_{norm} [%]	Δ_{norm} difference to baseline. [%]	σ_P [mm]
0	1	2.41		5.60	-	0.05
0	4	9.62	2.41	5.60	-	0.18
0	10	24.06		5.60	-	0.45
25	1	3.79		5.32	-0.27	0.06
25	4	15.15	3.79	5.32	-0.27	0.23
25	10	37.86		5.32	-0.27	0.57
50	1	4.91		5.81	0.21	0.08
50	4	19.63	4.91	5.81	0.21	0.33
50	10	49.06		5.81	0.21	0.82
75	1	6.37		8.57	2.98	0.16
75	4	25.47	6.37	8.57	2.98	0.63
75	10	63.68		8.57	2.98	1.57

It is possible to observe from the data presented in Table 4.1 that, for the case of the 25% of material removed, the Δ_{norm} difference to the baseline model it is almost zero. The same can be said for the case of 50% of material removed. Nevertheless, the model that has 75% of the spine removed in the spanwise direction, presents a significantly higher value of Δ_{norm}. This indicates that the use of cutouts do not have a significant effect in the deflection variation for value from 0 to a certain point where this effect starts to appear.

Looking at the standard deviation results (σ_P) for the models studied in this chapter, independently of percentages of material removed, the σ_P is always higher than the σ_P obtained for the baseline model. Translating these results it can be concluded that elastic washout increases with the use of cutouts in the spine. This confirms the expected behaviour when removing material from the spine which is to increase the elastic washout.

Another fact that can be stated from the data in Table 4.1 is that the cutouts with values of Δ_{norm} closest to the value presented by the baseline model is the 50% of removed material (Δ_{norm} difference to baseline ≈ 0). This model also presents high values for the difference between the model standard deviation of the baseline when compared to the same value for 25% but, significantly lower when compared to the ones presented by the 75% model.

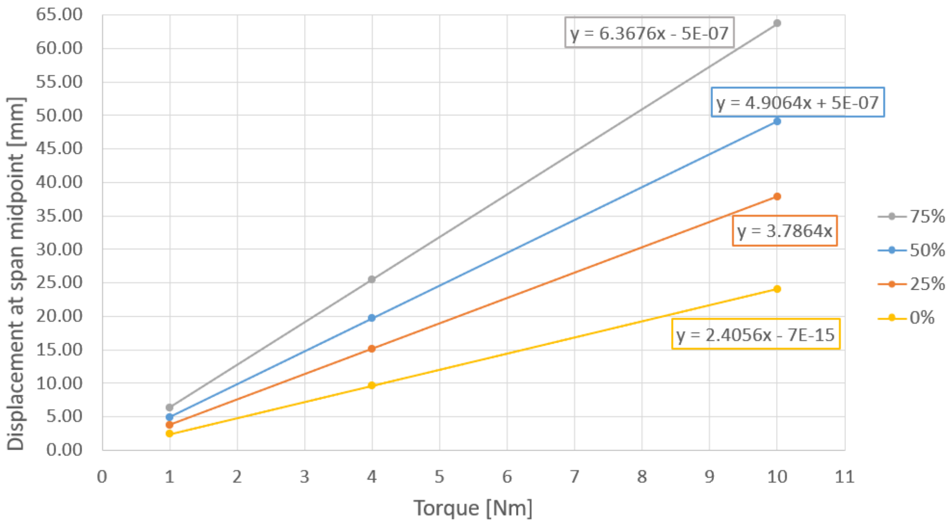

Figure 4.3: Displacement measured at the span midpoint in function of the applied T.

In Figure 4.3 it can be seen that, for the same applied T, the displacement for the span midpoint increases with the increase of the percentage of material removed. This behaviour was expected because, by removing material from the spine, we are decreasing the stiffness of the material allowing it to be more easily bent and achieve higher displacements. This is also confirmed by the slopes of the lines that represent the percentage of material removed. For a cutout with higher dimensions, the trailing edge reaches a specific deflection with less applied T. For example, to achieve 20 mm of displacement, the model with 75% of material removed only need an applied T of approximately 3.2 Nm, whereas the model with 50% needs 4 Nm, the 25% model a applied T of 5.4 Nm and the baseline 8.4 Nm. This reduction in the applied T, with the increase of the dimension of the cutouts, can be translated into less energy needed for the FishBAC device to function, with a reduced weight associated.

Figure 4.4 shows the effect of the dimension of the cutouts in the trailing edge displacement at the span midpoint, for different values of applied T. This representation can be used to estimate what will be the values of the trailing edge displacement for a given percentage of material removed from the spine in the spanwise direction, for the values of applied T and even for the values between. This can be used as a reference to begin the process of designing a FishBAC device.

For instance, in order to achieve 25 mm of deflection of the trailing edge, it can be said that a FishBAC model, similar to the one designed in this work, having almost no cutouts in the spine, will need an applied T of 10 Nm. This same model but with over 70% of spine removed in the spanwise direction will only need 4 Nm to achieve the 25 mm of deflection required.

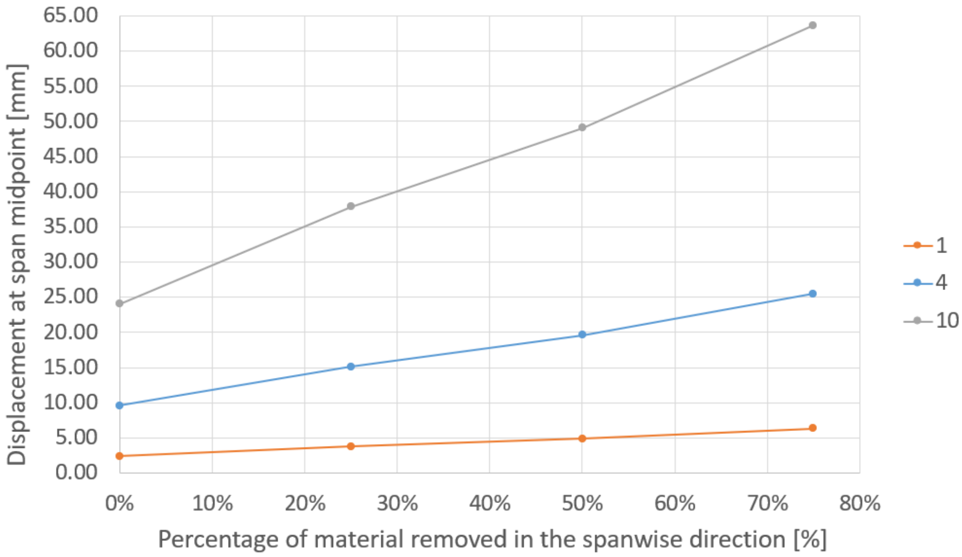

Figure 4.4: Effect of the cutouts in the displacement at span midpoint for different values of applied T.

A representation of the values of the (σ_P) and the Δ_{norm} for an applied T of 4Nm, considering the dimensions of the cutouts, is presented in Figure 4.5. With this representation, it is possible to say that the increase in the dimensions of the cutouts in the FishBAC's spine translates into an increase in both parameters that represent the elastic washout effect (σ_P and Δ_{norm}).

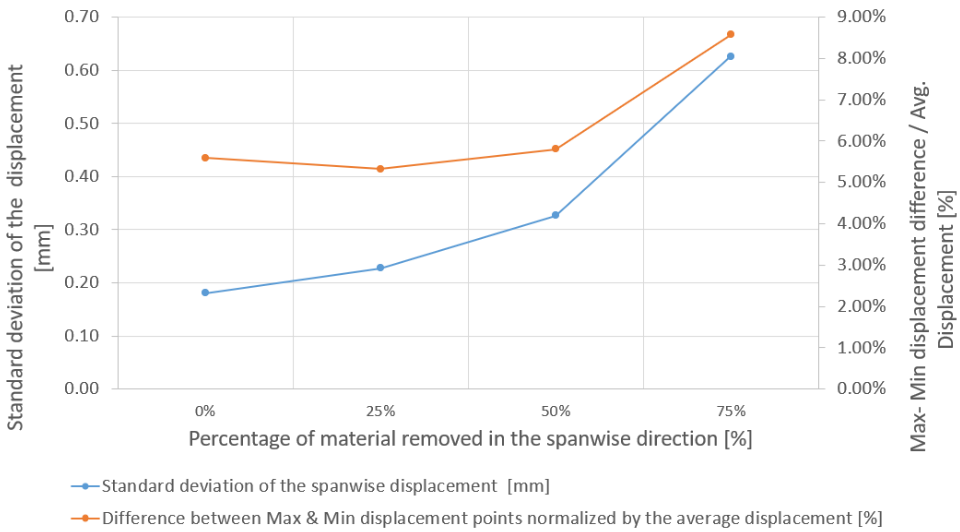

Figure 4.5: Effect of the Cutouts in the σ_P and the Δ_{norm} for 4 Nm.

Taking all of this into consideration, it is possible to say that 50% cutout configuration seems to provide the best balance of less rigidity, requiring less T for a specific displacement and not a significantly high elastic washout effect.

The full impact of removing spine material should ultimately be considered in an aeroelastic sense, in order to make sure that the reduced stiffness does not lead to any undesired aeroelastic phenomena, but that falls outside the scope of the present work.

4.2 Model B1

The model B1 that includes the CFRP pultrusions was designed starting from the baseline model.

To do the computational modelling of this structure, it is necessary to define the 1D lines where the CFRP pultrusions, which will be represented by 1D lines, will be placed. These lines were defined by the interception between the 2D planes that correspond to the stringers and the skin components. This will make sure that, when doing the computational testing, the pultrusions are still together to the skin and the stringer and in the right place.

The next step of the FEA for the B1 model was the creation of the 1D mesh for the previously defined pultrusion location lines. To achieve this it is necessary to inform the Siemens NX software what the element type is and what is the base size. In this case, the element selected was the CBAR. The CBAR element is a beam that supports tension and compression, torsion, bending in two perpendicular planes, and shear in two perpendicular planes, being adequate for the specific mechanical testing that will be performed after. This type of beam element has its formulation derived from classical beam theory also known as Euler-Bernoulli theory where the plane cross sections remain plane and normal to the longitudinal axis of the beam, during deformation.

In this step, the PBARL was used to define the physical properties of the material to establish what is the cross-section of the pultrusion to the software.

The Siemens NX gives the user a wide variety of cross-sections that can be used to define a specific material. In this case, a simple square bar was selected and the menu that the software provides is equal to the one presented in Figure 4.6. This type of cross section was selected because it is easier to fit in the junction between the stringers and the skin as these components make a 90 degrees angle where they meet.

As it can be seen, the user needs to define two dimensions, width (DIM1) and height (DIM2). For the purpose of the study, these dimensions (DIM1 and DIM2) are the same. What is relevant in this step is that the study that is going to be performed for model B1 is to change this dimension and see what effect it can produce. The selected measures that are being studied are 1 mm, 2 mm and 3 mm.

The value of 3 mm of base size was maintained and applied to this new 1D mesh.

In this process, the definition of the material was also very important because the Siemens NX Software does not have a typical unidirectional fibre-reinforced epoxy resin in the materials library. The material properties values used were taken from Agarwal et al. (2017) and are listed in the table 4.2. The material was defined as isotropic which, in this case, it is acceptable, considering that the pultrusion will act primarily as an axially loaded member, with transverse strains and stresses, not having a first order impact on the overall stiffness of the FishBAC.

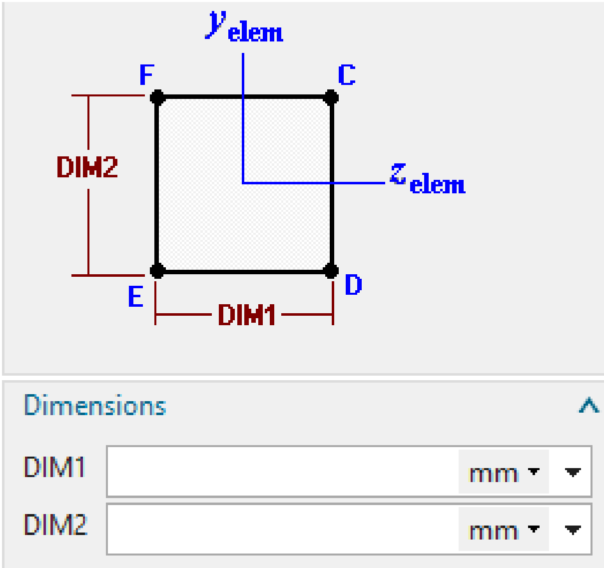

Figure 4.6: Cross section of the CFRP Pultrusion.

Table 4.2: Properties Graphite (adapted from Agarwal et al., 2017).

Property	**Graphite (Thornel300)**
Specific gravity	1.61
Tensile strength, 0^o (MPa)	1725
Tensile modulus, 0^o (GPa)	159
Tensile strength, 90^o (MPa)	42
Tensile modulus, 90^o (GPa)	10.9
In-plane shear strength (MPa)	95
In-plane shear modulus (GPa)	6.4
Longitudinal Poisson ratio (ν_{LT})	0.38

4.2.1 Obtained Results

The obtained results for the spanwise displacement with relation to the different CFRP pultrusion are summarised in Table 4.3. It is important to mention that the added mass that appears in Table 4.3 accounts for the mass of the CFRP pultrusions and it was computed by multiplying the specific gravity, presented in Table 4.2 by the cross-section area and by the span dimension.

As registered for the A1 model, the yield strength of the materials used was not reached being all the components of the structure in the linear elastic behaviour.

The model that uses the pultrusion with a 3×3 mm^2 squared cross-section has, as seen in Table 4.3, the highest value of the differences between the Δ_{norm} and the equivalent value observed in the model with no pultrusions. This is also true for the σ_P. Considering this, it is possible to say that the higher the cross-section area of the pultrusion, the less variation in the displacement of the trailing edge is registered and the less elastic washout verified in the model. This behaviour was expected since the pultrusion are highly rigid materials when compared to the materials used in the skin and stringers, having more capacity to distribute the loads along the span, when compared to skin and stringers without this feature.

Table 4.3: Results for the spanwise displacement with relation to the dimension of the cross-section of the Square pultrusion.

Dimension of cross-section Square pultrusion [mm]	T [Nm]	$w_{s/2}$ [mm]	Δ_{norm} [%]	Δ_{norm} difference to baseline. [%]	σ_P [mm]	Added Mass [g]	Reduction of Δ_{norm} / Added Mass [%/g]
0	1	2.41	5.60	-	0.05	-	-
0	4	9.62	5.60	-	0.18	-	-
0	10	24.06	5.60	-	0.45	-	-
1	1	2.41	5.31	-0.28	0.04	1.60	-0.18
1	4	9.63	5.31	-0.28	0.18	1.60	-0.18
1	10	24.07	5.31	-0.28	0.44	1.60	-0.18
2	1	2.41	5.25	-0.34	0.04	6.41	-0.05
2	4	9.62	5.25	-0.34	0.18	6.41	-0.05
2	10	24.06	5.25	-0.34	0.44	6.41	-0.05
3	1	2.41	5.19	-0.41	0.04	14.42	-0.03
3	4	9.62	5.19	-0.41	0.17	14.42	-0.03
3	10	24.06	5.19	-0.41	0.44	14.42	-0.03

It is important to mention that the inclusion of the pultrusions did not affect the ratio between the applied torque and the respective trailing edge displacement when compared to the results for the A1 model.

For this model, it is necessary to understand if the introduction of the mass associated with these CFRP reinforcements is significant. The three columns on the right side of Table 4.3 show metrics relating to the mass added. Analysing the values presented there, it is possible to conclude that the model that has 1 mm squared cross-section CFRP pultrusions has the best trade-off between reduction in the Δ_{norm} and the added mass. The same is verified for the parameter that relates the reduction in the σ_P and added mass.

Figure 4.7 shows the effect of the use of different dimensions for the cross-section of the pultrusions in the σ_P and the Δ_{norm} of the displacement difference for 4 Nm.

Both σ_P and Δ_{norm} with the increase of the dimensions of the cross-section of the square pultrusion, have a really modest negative tendency that can be verified in figure 4.7. This support the affirmation that the added pultrusions have a low effect on preventing the elastic washout to happen, with only a very modest reduction in the variation of the trailing edge deflection along the span. This can be the real behaviour of a model with these features but, it can not be excluded that the modelling approach can also be influencing these results.

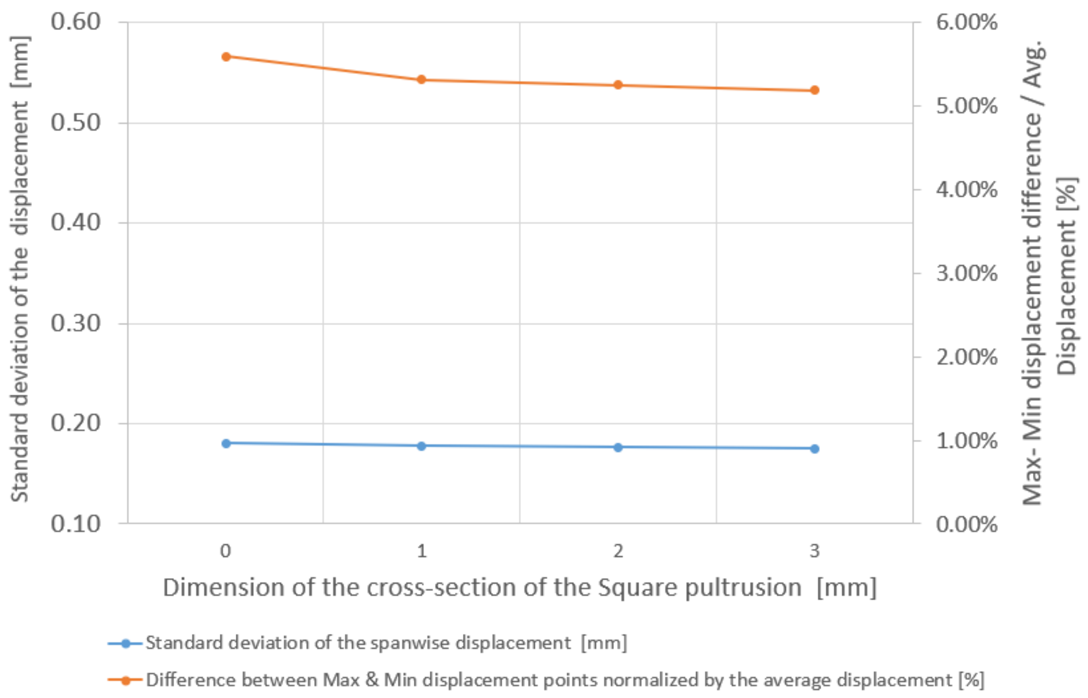

Figure 4.7: Effect of the pultrusions in the σ_P and the Δ_{norm} for an applied T of 4 Nm.

4.3 Model combining A1 and B1

Considering the promising results obtained for the previously studied models, a third model that combines the two other was created and studied.

The configurations studied were the combination of cutouts with 50% of material removed with a 1 mm and 2 mm squared CFRP pultrusion. Also, the models that combine cutouts with 75% material removed with the 1 mm and 2 mm squared CFRP pultrusion were designed and analysed.

The cutouts with 50% of material spine removed were selected to be used in the combining model, due to the fact that the model with this characteristic presented the best trade-off between the quantity of material removed and percentage of the variation in displacement along the span.

The model with 75% of material removed was also selected in order to understand if the pultrusion could affect the really high variation shown in Table 4.1. The expected results for the combination of these with CFRP pultrusions is to lower the values of variation in trailing edge displacement. It is going to be analysed if the respective results could be approximated to the one obtained for the model with no cutouts.

4.3.1 Obtained Results

The obtained results for the combined model are presented in Table 4.4.

From the data presented in table 4.4 it is possible to state that both types of pultrusions tested in the combination with cutouts with 75% material removed have reduced the variation in the displacement. Although, this reduction was not significant to be approximated to the results obtained for the model with no cutouts, not meeting the expectations defined in the chapter 4.3. Even though, it is important to

Table 4.4: Obtained results from Model combining A1 and B1

% of material removed in spanwise direction [%]	Dimension of the cross-section of Square pultrusion [mm]	T [Nm]	$w_{s/2}$ [mm]	Δ_{norm} [%]	Δ_{norm} difference to baseline. [%]	σ_P [mm]	Added Mass [g]	Reduction of Δ_{norm} / Added Mass [%/g]	Reduction of the σ_P / Added Mass [%/g]
50	1	1	4.88	5.73	0.13	0.08	1.60	0.08	48.16
50	1	4	19.53	5.73	0.13	0.32	1.60	0.08	48.16
50	1	10	48.83	5.73	0.13	0.80	1.60	0.08	48.16
50	2	1	4.87	5.54	-0.06	0.08	6.41	-0.01	11.25
50	2	4	19.50	5.54	-0.06	0.31	6.41	-0.01	11.25
50	2	10	48.74	5.54	-0.06	0.78	6.41	-0.01	11.25
75	1	1	6.34	8.32	2.72	0.15	1.60	1.70	144.08
75	1	4	25.38	8.32	2.72	0.60	1.60	1.70	144.08
75	1	10	63.44	8.32	2.72	1.49	1.60	1.70	144.08
75	2	1	6.34	8.00	2.40	0.14	6.41	0.37	33.43
75	2	4	25.38	8.00	2.40	0.57	6.41	0.37	33.43
75	2	10	63.45	8.00	2.40	1.42	6.41	0.37	33.43

mention that the CFRP pultrusions with 2 mm squared cross-section had better results when compared to the ones obtained for 1 mm.

A major conclusion of the combined model study is that applying 2 mm pultursions in the model with the 50% cutout gives an outstanding result that is capable of achieving twice the trailing edge deflection verified in the baseline model (48.74 mm vs 24.06 mm) and also slightly improve the displacement variation in spanwise direction (5.54% vs 5.6%).

This model is also the one that shows the lowest value, from the studied ones, for the parameters that are related to the added mass (reduction of the Δ_{norm} divided by the added mass and reduction of the σ_P divided by the added mass).

Chapter 5

Conclusions

5.1 Achievements

The main objective of this dissertation was to propose new structural solutions that could respond to the limitations of the existing model of the FishBAC device. Firstly, a study was conducted in order to understand the basic structural concepts in play, as well as the steps to perform a FEM analysis.

At this point, the existing knowledge of camber morphing wings and the FishBAC was reviewed.

Brainstorming was done in order to have conceptual ideas of what possible solution could be implemented. With the conceptual ideas established, a decision process was used in order to choose the concepts that were more promising to better respond to the improving objectives of the FishBAC. From this step, it was concluded that the modifications to be studied were the introduction of cutouts in the spine (Model A1) and the reinforcement of the stringers, next to the skin, using CFRP pultrusions (Model B1)

Then, a CAD model representation of the FishBAC was designed. The FEA was applied to this model, the respective results were registered and later used as the baseline of the study of the modifications. A mesh convergence test was conducted. From this, it was concluded that the mesh did not converge.

Finally, the modifications were studied beginning with A1 model. The results obtained helped to conclude that, removing some of the spine's material in rectangular cutouts can reduce the total mass and energy required to achieve a specific deflection.

One other conclusion possible for this modification was that, the use of cutouts reduces the bending stiffness of the device, increasing displacement at a given T. But, if too much is removed, a higher percentage variation in displacement along the span starts to occur. The cutouts that remove 50% of the spine in the spanwise direction look to provide the best balance of these factors.

Next in this study was the assessment of model B1 and it was concluded that introducing CFRP pultrusion connected to the stringer, next to the skin, has a minor but positive effect in the reduction of the spanwise variation.

As conclusions for the combination of the models A1 and B1, it was found that combining 2 mm pultrusions in the model with the 50% cutout in the spanwise direction, although it is a model that has less rigidity, it can deliver a deflection that is two times more than the deflection obtained for the baseline model. This configuration of pultrusion and cutouts was found to have less variation in the spanwise direction. It was also concluded that this model (2 mm pultrusions in the model with the 50% cutout) is also the one that shows the lowest value, from the studied ones, for the parameters that are related to the added mass (reduction of the Δ_{norm} divided by the added mass and reduction of the σ_P divided by the added mass).

5.2 Limitations

One of the limitations felt was associated with the FEA process which had showed to be more challenging than expected. Firstly, the baseline obtained mesh did not pass the convergence test despite the various meshes and processes for its generation that, in same cases, lead to great computational work and long runtimes.

Then, it was also challenging the achievement of a well-secured connection between the 2D Shell, 2D Shell laminated elements and 3D Solid elements, due to the lack of information available for the software used. This involved a process of trying multiple computational options in the Siemens NX and validations until a solution was found.

The obtained results can be limited by the meshing/modelling, for instance, the effectiveness of model B1 in the reduction of the spanwise deflection variation.

Despite all computational limitations, it can be stated that the conclusions are of high relevancy because the evaluated performance is always done, having the baseline as a reference.

5.3 Future Work

The work was carried out with the certainty that this is a field that still has a lot to study and develop but that could be very promising and bring positive changes in relation to the aircraft models we know today.

The continuation of this work will be important to help the evolution of the FishBAC in terms of performance and efficiency in the achievement of the design objectives of this type of camber morphing device.

An economic, maintenance and operation study, to assess the potential of the solutions proposed, can be a future work that could help the implementation of this technology in real operating aircraft wings.

Another possible work to be done is to do a study of other types of shapes for the cutouts and cross-section of the pultrusions. It is also crucial to study an effective way for the insertion of the CFRP pultrusions next to skin and stringers. To overcome some of the difficulties and limitations encountered it is proposed to redo the process of generating the mesh and the converging test.

Finally, it is suggested to do a real-life application of the model, by building a prototype and then, do a real mechanical test to validate the results obtained and the drawn conclusions.

Bibliography

Agarwal, B. D., Broutman, L. J., & Chandrashekhara, K. (2017). *Analysis and performance of fiber composites*. Wiley.

Airfoil Tools. (2022). *Naca 23012 12% (naca23012-il).* Retrieved 2022-07-26, from `http://airfoiltools.com/airfoil/details?airfoil=naca23012-il`

Barbarino, S., Bilgen, O., Ajaj, R. M., Friswell, M. I., & Inman, D. J. (2011, June). A review of morphing aircraft. *Journal of Intelligent Material Systems and Structures*, *22*(9), 823–877. Retrieved from `https://doi.org/10.1177/1045389x11414084` doi: 10.1177/1045389x11414084

Barbarino, S., Pecora, R., Lecce, L., Concilio, A., Ameduri, S., & Calvi, E. (2009, August). A novel sma-based concept for airfoil structural morphing. *Journal of Materials Engineering and Performance*, *18*, 696-705. doi: 10.1007/s11665-009-9356-3

Barros, A. F. M. (2018). *Simetria materiais - mecânica dos sólidos*. Secção de Folhas - Instituto Superior Técnico.

Beer, F. P., & Johnston, E. R. (2012). *Mechanics of materials* (6th ed.). McGraw-Hill.

Bilgen, O., Friswell, M., Kochersberger, K., & Inman, D. (2011, April). Surface actuated variable-camber and variable-twist morphing wings using piezocomposites. In *52nd AIAA/ASME/ASCE/AHS/ASC structures, structural dynamics and materials conference.* American Institute of Aeronautics and Astronautics. Retrieved from `https://doi.org/10.2514/6.2011-2072` doi: 10.2514/6.2011-2072

Biswas, K. (2020, February). Military aviation principles. In *Military engineering.* IntechOpen. Retrieved from `https://doi.org/10.5772/intechopen.87087` doi: 10.5772/intechopen.87087

Brandt, S. A., Stiles, R. J., Bertin, J. J., & Whitford, R. (2015). *Introduction to aeronautics: A design perspective* (3th ed.). AIAA EDUCATION SERIES.

Burdette, D. A., & Martins, J. R. R. A. (2019). Impact of morphing trailing edges on mission performance for the common research model. *Journal of Aircraft*, *56*, 369-384. doi: 10.2514/1.C034967

Daynes, S., Nall, S. J., Weaver, P. M., Potter, K. D., Margaris, P., & Mellor, P. H. (2010, January). Bistable composite flap for an airfoil. *Journal of Aircraft*, *47*(1), 334–338. Retrieved from `https://doi.org/10.2514/1.45389` doi: 10.2514/1.45389

Esposito, E., & Raffa, L. (2007, January). Global reorganisation in a high-technology industry: The aircraft industry. *International Journal of Globalisation and Small Business*, *2*. doi: 10.1504/IJGSB.2007.015480

Gaspari, A., & Ricci, S. (2010, June). A two levels approach for the optimal design of morphing airfoils. In *13th AIAA/ISSMO multidisciplinary analysis optimization conference.* American Institute of Aeronautics and Astronautics. Retrieved from https://doi.org/10.2514/6.2010-9388 doi: 10.2514/6.2010-9388

Gaspari, A., Ricci, S., & Riccobene, L. (2014, October). Design, manufacturing and wind tunnel validation of an active camber morphing wing based on compliant structures. In *25th international conference on adaptive structures and technologies.* The Hague, The Netherlands: American Institute of Aeronautics and Astronautics.

Greff, E. (1990). The development and design integration of a variable camber wing for long/medium range aircraft. *The Aeronautical Journal (1968)*, *94*(939), 301–312. doi: 10.1017/S0001924000023186

Heeb, R. M., Dicker, M., & Woods, B. K. S. (2022, September). Design space exploration and modelling of GATOR 3d printed morphing skins. In *ASME 2022 conference on smart materials, adaptive structures and intelligent systems.* American Society of Mechanical Engineers. Retrieved from https://doi.org/10.1115/smasis2022-93488 doi: 10.1115/smasis2022-93488

Hibbeler, R. C. (2017). *Mechanics of materials* (10th ed.). Pearson.

Kota, S., Hetrick, J. A., Osborn, R., Paul, D., Pendleton, E., Flick, P., & Tilmann, C. (2003, August). Design and application of compliant mechanisms for morphing aircraft structures. In E. H. Anderson (Ed.), *SPIE proceedings.* SPIE. Retrieved from https://doi.org/10.1117/12.483869 doi: 10.1117/12.483869

Kudva, J. N. (2004, April). Overview of the DARPA smart wing project. *Journal of Intelligent Material Systems and Structures*, *15*(4), 261–267. Retrieved from https://doi.org/10.1177/1045389x04042796 doi: 10.1177/1045389x04042796

Larson, R. R. (1986). *Flight control system development and flight test e:xperience with the f·11-1 mlission adaptive wing aircraft* (Tech. Rep.).

MatWeb. (2022). *Aluminum 2014-o.* Retrieved 2022-07-28, from https://www.matweb.com/search/DataSheet.aspx?MatGUID=3380dbc77437443b9674c6da219bd664&ckck=1

Milojević, A. P., & Pavlović, N. D. (2016, June). Development of a new adaptive shape morphing compliant structure with embedded actuators. *Journal of Intelligent Material Systems and Structures*, *27*, 1306-1328. doi: 10.1177/1045389X15590270

Molinari, G., Quack, M., Dmitriev, V., Morari, M., Jenny, P., & Ermanni, P. (2011, July). Aero-structural optimization of morphing airfoils for adaptive wings. *Journal of Intelligent Material Systems and Structures*, *22*, 1075-1089. doi: 10.1177/1045389X11414089

Monner, H., Kintscher, M., Lorkowski, T., & Storm, S. (2009, May). Design of a smart droop nose as leading edge high lift system for transportation aircrafts. In *50th AIAA/ASME/ASCE/AHS/ASC structures, structural dynamics, and materials conference.* American Institute of Aeronautics and Astronautics. Retrieved from https://doi.org/10.2514/6.2009-2128 doi: 10.2514/6.2009-2128

Niu, M. C.-Y. (1999). *Airframe - stress analysis and sizing* (2nd ed.). Conmilit Press LTD.

Previtali, F., G.Molinari, Arrieta, A. F., Guillaume, M., & Ermanni, P. (2016, January). Design and experimental characterisation of a morphing wing with enhanced corrugated skin. *Journal of Intelligent Material Systems and Structures*, *27*, 278-292. doi: 10.1177/1045389X15595296

Ramos, M. H. S. (2015). *Construction and analysis of a lightweight UAV wing prototype aerospace engineering examination committee* (Master's thesis, Instituto Superior Técnico). Retrieved from https://fenix.tecnico.ulisboa.pt/downloadFile/1126518382177896/MarioRamos_Thesis.pdf

Raymer, D. (2018). *Aircraft design: A conceptual approach* (6th ed.). AIAA EDUCATION SERIES.

Reddy, J. (2003). *Mechanics of laminated composite plates and shells - theory and analysis* (2nd ed.). CRC Press LLC.

Rivero, A. E., Fournier, S., Heeb, R., & Woods, B. K. S. (2022, January). Design, manufacture and wind tunnel test of a modular fishbac wing with novel 3d printed skins. *Applied Sciences (Switzerland)*, *12*. doi: 10.3390/app12020652

Rivero, A. E., Fournier, S., Manolesos, M., Cooper, J., & Woods, B. K. S. (2020, January). Wind tunnel comparison of flapped and FishBAC camber variation for lift control. In AIAA Scitech 2020 Forum (Ed.), . Orlando, FL: American Institute of Aeronautics and Astronautics, Inc. doi: 10.2514/6.2020-1300

Rivero, A. E., Fournier, S., Manolesos, M., Cooper, J. E., & Woods, B. K. S. (2021, July). Experimental aerodynamic comparison of active camber morphing and trailing-edge flaps. *AIAA Journal*, *59*, 2627-2640. doi: 10.2514/1.J059606

Rivero, A. E., Fournier, S., Weaver, P., Cooper, J. E., & Woods, B. K. S. (2018, October). Manufacturing and characterisation of a composite FishBAC morphing wind tunnel model. In 29th International Conference on Adaptive Structures and Technologies, ICAST 2018 (Ed.), . Retrieved from http://www.icast2018.com

Rivero, A. E., Weaver, P., Cooper, J. E., & Woods, B. K. S. (2018, May). Parametric structural modelling of fish bone active camber morphing aerofoils. *Journal of Intelligent Material Systems and Structures*, *29*, 2008-2026. doi: 10.1177/1045389X18758182

Roylance, D. (2000). Stresses in beams. *Department of Materials Science and Engineering MIT*, 1–18.

Shape adaptive blades for rotorcraft efficiency. (2021, June). Retrieved from https://sabreproject.eu/#header

Sofla, A. Y. N., Meguid, S. A., Tan, K. T., & Yeo, W. K. (2010, March). Shape morphing of aircraft wing: Status and challenges. *Materials &amp Design*, *31*(3), 1284–1292. Retrieved from https://doi.org/10.1016/j.matdes.2009.09.011 doi: 10.1016/j.matdes.2009.09.011

Systèmes, D. (2017, April). Solidworks manual 2017 [Computer software manual]. Retrieved from http://help.solidworks.com/2017/english/SolidWorks/SWHelp_List.html?id=dd61f48c463f46c499c3946503773821#Pg0&ProductType=&ProductName=

Thill, C., Etches, J., Bond, I., Potter, K., & Weaver, P. (2008, March). Morphing skins. *The Aeronautical Journal*, *112*(1129), 117–139. Retrieved from https://doi.org/10.1017/s0001924000002062 doi: 10.1017/s0001924000002062

Valasek, J. (2012). *Morphing aerospace vehicles and structures* (Vol. 57). John Wiley & Sons.

Vasista, S., Riemenschneider, J., Kamp, B. V. D., Monner, H. P., Cheung, R. C., Wales, C., & Cooper, J. E. (2017). Evaluation of a compliant droop-nose morphing wing tip via experimental tests. *Journal of Aircraft*, *54*, 519-534. doi: 10.2514/1.C033909

Vasista, S., Tong, L., & Wong, K. C. (2012, January). Realization of morphing wings: A multidisciplinary challenge. *Journal of Aircraft*, *49*(1), 11–28. Retrieved from https://doi.org/10.2514/1.c031060 doi: 10.2514/1.c031060

Woods, B. K. S., Fincham, J. H. S., & Friswell, M. I. (2014). Aerodynamic modelling of the fish bone active camber morphing concept. In *Proceedings of the raes applied aerodynamics conference, bristol, uk* (Vol. 2224).

Woods, B. K. S., & Friswell, M. I. (2012, September). Preliminary investigation of a fishbone active camber concept. In *Volume 2: Mechanics and behavior of active materials integrated system design and implementation bio-inspired materials and systems energy harvesting.* American Society of Mechanical Engineers. Retrieved from https://doi.org/10.1115/smasis2012-8058 doi: 10.1115/smasis2012-8058

Woods, B. K. S., & Friswell, M. I. (2013, April). Fluid-structure interaction analysis of the fish bone active camber mechanism. In *54th AIAA/ASME/ASCE/AHS/ASC structures, structural dynamics, and materials conference.* American Institute of Aeronautics and Astronautics. Retrieved from https://doi.org/10.2514/6.2013-1908 doi: 10.2514/6.2013-1908

Woods, B. K. S., & Friswell, M. I. (2014, January). Structural characterization of the fish bone active camber morphing airfoil. In *22nd AIAA/ASME/AHS adaptive structures conference.* American Institute of Aeronautics and Astronautics. Retrieved from https://doi.org/10.2514/6.2014-1122 doi: 10.2514/6.2014-1122

Çınar, K., Ozturk, U., Ersoy, N., & Wisnom, M. (2014, February). Modelling manufacturing deformations in corner sections made of composite materials. *Journal of Composite Materials*, *48*. doi: 10.1177/0021998313477896